



BIOMEDICA: An Open Biomedical Image-Caption Archive, Dataset, and Vision-Language Models Derived from Scientific Literature

Alejandro Lozano*

Department of Biomedical Data Science
Stanford University
lozanoe@stanford.edu

Min Woo Sun*

Department of Biomedical Data Science
Stanford University
minwoos@stanford.edu

James Burgess*

ICME
Stanford University
jmhb@stanford.edu

Liangyu Chen

Department of Computer Science
Stanford University
liangyuc@stanford.edu

Jeffrey J. Nirschl

Department of Pathology
Stanford University
jnirschl@stanford.edu

Jeffrey Gu

ICME
Stanford University
sanketg@stanford.edu

Ivan Lopez

Department of Biomedical Data Science
Stanford University
ivlopez@stanford.edu

Josiah Aklilu

Department of Biomedical Data Science
Stanford University
josaklil@stanford.edu

Anita Rau

Department of Biomedical Data Science
Stanford University
arau@stanford.edu

Austin Wolfgang Katzer

Department of Developmental Biology
Stanford University
awkatzer@stanford.edu

Yuhui Zhang

Department of Computer Science
Stanford University
yuhuiz@stanford.edu

Collin Chiu

Department of Biochemistry
Stanford University
cochiu9@stanford.edu

Xiaohan Wang

Department of Biomedical Data Science
Stanford University
xhanwang@stanford.edu

Alfred Seunghoon Song

Department of Biomedical Data Science
Stanford University
alfredss@stanford.edu

Robert Tibshirani

Department of Biomedical Data Science
Department of Statistics
Stanford University
tibs@stanford.edu

Serena Yeung-Levy

Department of Biomedical Data Science
Department of Electrical Engineering
Department of Computer Science
Stanford University
syyeung@stanford.edu

Abstract

The development of vision-language models (VLMs) is driven by large-scale and diverse multi-modal datasets. However, progress toward generalist biomedical VLMs is limited by the lack of annotated, publicly accessible datasets across biology and medicine. Existing efforts are limited to narrow domains, missing the full diversity of biomedical knowledge encoded in scientific literature. To address this gap, we introduce *BIOMEDICA*: a scalable, open-source framework to extract, annotate, and serialize the entirety of the PubMed Central Open Access subset into an easy-to-use, publicly accessible dataset. Our framework produces a comprehensive archive with over 24 million unique image-text pairs from over 6 million articles. Metadata and expert-guided annotations are additionally provided.

We demonstrate the utility and accessibility of our resource by releasing *BMCA-CLIP*, a suite of CLIP-style models continuously pre-trained on *BIOMEDICA* dataset via streaming (eliminating the need to download 27 TB of data locally). On average, our models achieve state-of-the-art performance across 40 tasks — spanning pathology, radiology, ophthalmology, dermatology, surgery, molecular biology, parasitology, and cell biology — excelling in zero-shot classification with 6.56% average improvement (as high as 29.8% and 17.5% in dermatology and ophthalmology, respectively) and stronger image-text retrieval while using 10x less compute. To foster reproducibility and collaboration, we release our codebase^{1,2} and dataset³ for the broader research community.

1. Introduction

Progress in vision-language foundation models (FMs) is driven by readily available large-scale and diverse datasets [16, 49]. Providing the basis for pretraining and adaptation, leading to strong visual representations, and achieving expert-level zero-shot performance across a wide range of downstream tasks [3, 53, 62].

This success in the general domain has sparked interest in biomedical multimodal FMs as integrating knowledge captured throughout different modalities across medical specialties, molecular biology, genetics, and related fields has the potential to revolutionize precision health. For instance, in daily practice, clinicians typically have one care-related question for every two patients seen [15], often turning to sources like UpToDate for summarized information to address these inquiries [14]. Questions that cannot be answered within three minutes are often aban-

¹<https://github.com/minwoosun/biomedica-etl>

²https://github.com/Ale9806/open_clip_with_biomedica

³<https://huggingface.co/BIOMEDICA>

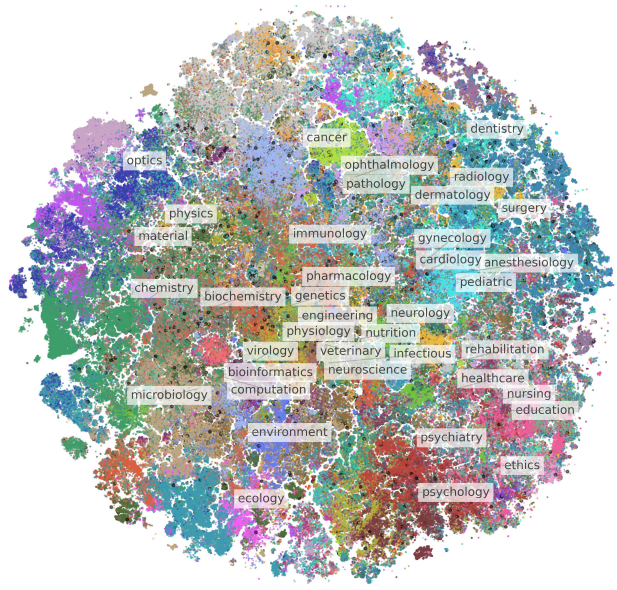


Figure 1. **Overlap of BIOMEDICA dataset with the Landscape of Biomedical Research** [22] Each color and labeled region reflects thematic concentrations, capturing the diversity of topics within our dataset. Gray points represent articles not present in our dataset.

doned, negatively impacting patient care [15, 37]. Biomedical FMs could bridge this gap by retrieving relevant information from visual and textual findings – linking observations to emerging therapeutics, providing additional recommendations (e.g. linking a patient to a promising clinical trial [29, 58]), flagging missed diagnoses [47], and identifying biomarkers correlated with patient prognosis [23] – ultimately offering essential support for patient care and informed medical decision-making.

However, despite the growing interest in generalist biomedical FMs [39], the pursuit of this goal is hindered by the limited availability of **annotated** and **publicly accessible** multimodal datasets **across a wide array of biomedical domains**.

Furthermore, privacy concerns associated with sharing patient information [21] and the logistical complexities of expert-level annotation exacerbates data collection, annotation, and redistribution at scale [61].

Scientific biomedical literature, however, provides an ever-expanding, highly curated multimodal resource encompassing the knowledge of specialized professionals, reflecting rigorously supported medical and biological evidence. Naturally, open-source biomedical literature offers an unparalleled resource to construct comprehensive and diverse datasets at scale.

PubMed [46], a free archive of biomedical and life sci-

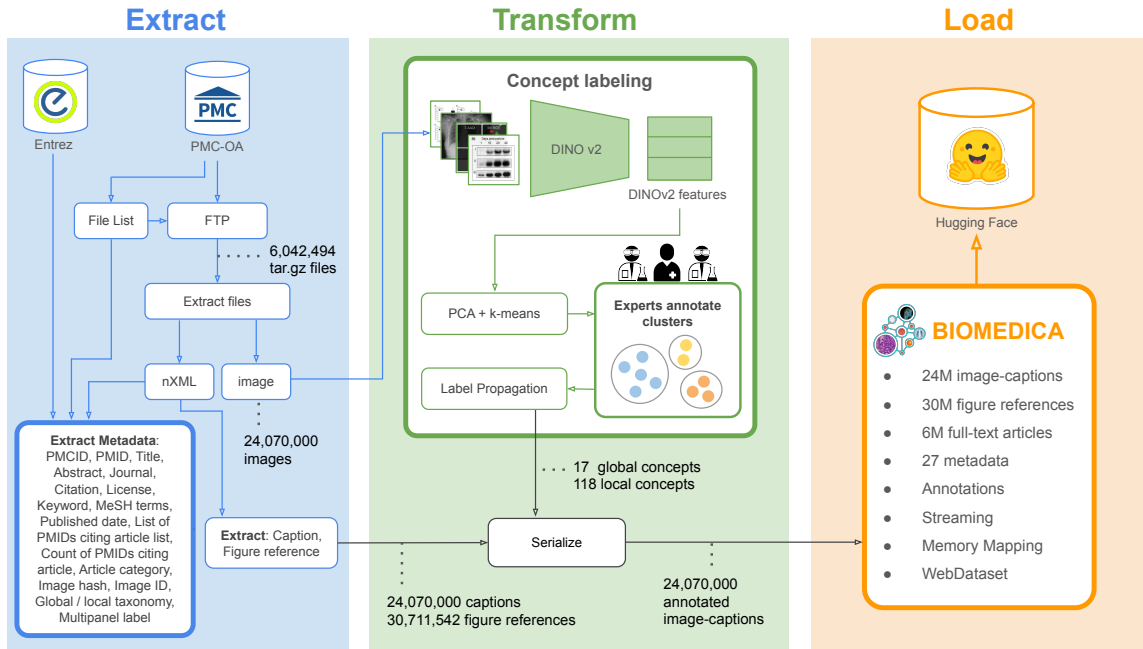


Figure 2. **BIOMEDICA curation pipeline:** In the Extract phase, metadata, text (caption, figure reference, full-text), and images are sourced and processed from PMC-OA. In the Transform phase, DINO v2 features are generated for each image, followed by clustering using PCA and k-means. Clinicians and scientists annotate these clusters, identifying 12 global concepts and 170 local concepts, which are then propagated across all images. Finally, in the Load phase, the dataset is made available on Hugging Face with the listed features.

ences literature, indexes approximately 1.5 million new publications annually—equivalent to over two papers per minute—with a 9% yearly growth rate. While prior efforts have leveraged this resource [34, 43, 51], current open-source literature-based biomedical datasets are often pre-filtered to narrow diagnostics imaging modalities within radiology and pathology, overlooking the vast breadth of complementary information available in other fields such as cell and molecular biology, proteomics, omics, and pharmacogenomics [38]. These adjacent domains provide insights into the very biological mechanisms that dictate health outcomes. Often, advancements in these areas lead to scientific discoveries that not only expand our understanding of complex biological processes but also influence medical practice (e.g. codeine super metabolizers: patients who metabolise codeine very rapidly are at increased risk of developing adverse effects [7]). Therefore, integrating knowledge from these domains is essential for effective clinical reasoning, yet it is often underappreciated in the development of biomedical vision-language training paradigms and datasets.

With the aim to democratize access to open-source scientific data across the vast landscape of biomedical research, we developed the **Biomedical Image-Caption Archive (BIOMEDICA)**, an **open-source framework** including: an ETL pipeline to efficiently extract and serialize

the entirety of PubMed Central Open Access (PMC-OA) repository into a standardized and dense archive, as well as tools to annotate, filter, and retrieve the archive on demand. Leveraging BIOMEDICA, we present the following contributions:

- **BIOMEDICA Dataset:** A large-scale, deep-learning-ready biomedical dataset containing over 24M image-caption pairs and 30M image-references from 6M unique open-source articles. Each data point is highly annotated with over 27 unique metadata fields, including article-level information (e.g., license, publication title, date, PMID, keywords, MeSH terms) and coarse-grained image metadata (e.g., primary and secondary content labels and panel type) assigned via an unsupervised algorithm and human curation by seven experts. The dataset is optimized for model development and is available in a hybrid format: Parquet [56] for fast querying and filtering, and WebDataset for high-throughput streaming (providing 3x-10x higher I/O rates when compared to random access memory). Table 1 summarizes the BIOMEDICA dataset, highlighting its distinctions from existing literature-based datasets.
- **BMCA-LIP:** We continually pretrain CLIP using the BIOMEDICA dataset. We leverage our features and tools, such as streaming (enabling remote training) and fast filtering, to explore modern training strategies, in-

Dataset	Scientific Papers	Image-Captions	Metadata Fields	Source	Streaming	Expert Curated Concepts
ROCO [43]	1.8M	0.08M	3	PMC-OA	×	×
MEDICAT [51]	1.8M	0.21M	3	PMC-OA	×	×
PMC-OA [34]	2.4M	1.65M	0	PMC-OA	✓	×
PMC-15M [67]	3M	15M	3	PMC-OA	×	×
BIOMEDICA(Ours)	6M	24M	27*	PMC-OA	✓	Clinicians & Scientists

Table 1. Comparison of our work to existing literature-based biomedical datasets. BIOMEDICA stands out by offering 2x more scientific papers and 1.6x more image-caption pairs, metadata fields, support for streaming, and expert-curated concepts from clinicians and scientists. *See Table 2 for a full list of provided metadata.

cluding concept filtering [20] and balancing [5].

- **Large-scale evaluation:** We standardized 40 established biomedical datasets across cell and molecular biology, radiology, pathology, ophthalmology, dermatology, and surgery to evaluate our models and compare them to prior work. Our assessments encompass zero-shot classification, image-to-text retrieval, and text-to-image retrieval. Leveraging this benchmark, we observe that our best model surpasses previous state-of-the-art in two-thirds of the cases, achieving an average improvement of 6.56% in general biomedical imaging classification tasks and 6.7% in microscopy composition identification. Furthermore, our high-throughput dataset enables our models to outperform the current state-of-the-art with 10x less compute.

Our dataset and models are hosted on Hugging Face and will be updated annually to keep pace with the growing availability of biomedical data.

2. Related Work

Literature-based Biomedical Image-caption Pretraining

Datasets Biomedical image-caption pretraining mixtures leverage scientific literature to create pre-filtered datasets. Pelka et al. [43] leveraged PMC-OA subset [46] to develop the Radiology Objects in Context (ROCO) dataset. It filters PMC-OA images using a supervised CNN to classify and select radiology-specific images. This results in a collection of 81,000 image-caption pairs spanning seven radiology modalities, with additional annotations including keywords, UMLS identifiers, and semantic types. MEDICAT [51] extends ROCO by further filtering more medical images through a two-step process. First, a keyword filter searches for modality words (e.g., MRI, ultrasound) to identify medical images across captions and reference text. Next, a supervised ResNet-50 discards non-medical images. This results in 217,000 caption-figure pairs from 131,000 open-access biomedical papers. PMC-OA dataset [34] follows the same two-step filtering strategy as MEDICAT but replaces the ResNet-50 with a ResNet-101 model trained on the DocFigure dataset [30]. This approach yields 381,096 unique medical figures from 2.4 million articles, which are further refined into 1.65 million image-caption pairs. PMC-15M [67] scales literature-based biomedical datasets to 3

million articles, extracting 15 million image-caption pairs using PubMed Parser [2].

In contrast to prior work, (1) we adopt a domain-agnostic approach. Rather than filtering to specific domains, we provide 9x more metadata and expert-derived annotations at various granularities. Subsequently, we offer a parallelized pipeline to use these metadata and filter subsets on demand, accommodating to different interests in the biomedical community. (2) Prior efforts rely on supervised models to classify images. An approach confounded by the diversity of the training datasets. Instead, we employ a multi-step, data-driven strategy guided by clinicians and scientists to (2.a) develop a comprehensive hierarchical taxonomy derived from biomedical ontologies and PMC-OA content, (2.b) annotate clusters of images following this taxonomy, and (2.c) propagate these annotations to each individual image. This data-centric approach ensures scalability, allowing newly added images to inherit labels from the nearest annotated data point.

Literature-based Biomedical Contrastive Pretraining

Large-scale, literature-based datasets enable self-supervised learning (SSL). PMC-CLIP [18] leverages one million image-caption pairs from PMC-OA to train an image-captioning model with a dual contrastive learning and masked language modeling objective. BiomedCLIP [67] expands on PMC-CLIP by pertaining on 15 million image-caption pairs from PMC-15M and upgrading the vision encoder to vision transformer (ViT-B-16).

Unlike the original CLIP model [45], prior work in the biomedical literature aligns vision-text representations from scratch with at least 8x smaller batch sizes and 26x smaller datasets – factors linked to suboptimal model performance [13, 33, 66]. Recognizing that even at 24M image-caption pairs, biomedical datasets are orders of magnitude smaller than general vision-language datasets (e.g., LAION-5B [49]) and the scarcity of large compute clusters in academia, we instead investigate continual pretraining. This setup, combined with our framework, enables the exploration of modern training techniques such as data filtering, data balancing, and robust fine-tuning [59].

Evaluation of Biomedical Image-caption Models While biomedical CLIP-style models may be trained on diverse

datasets, their evaluation is typically limited to tasks within radiology and pathology, overlooking the broader biomedical domain. In general, CLIP-style models are evaluated on retrieval, classification, and open vision-question answering (VQA) tasks. BiomedCLIP evaluates retrieval performance on a 726k held-out set from PMC-15M, with classification capabilities tested on LC25000 [9], Path-Camelyon [55], TCGA-TIL, and the RSNA 2018 Challenge [50]. PMC-CLIP assesses retrieval performance on ROCO [43] and classification performance on MedMNIST [64] (including PneumoniaMNIST, BreastMNIST, and DermMNIST). Both BiomedCLIP and PMC-CLIP also evaluate open-VQA performance on the VQA-RAD and Slake datasets. However, to support open-ended evaluation, additional models are included, requiring full training. BiomedCLIP introduces a transformer-based co-attention multimodal module that generates cross-modal representations from image and text encodings, which are then passed to a classifier to predict the final answer. In contrast, PMC-CLIP uses Model-Agnostic Meta-Learning (MAML) networks for its approach.

Existing evaluation protocols have several limitations. First, evaluations are narrow in scope as performance is quantified on a limited range of datasets, mainly radiology and pathology. Second, open-VQA evaluation relies on training at least one additional decoder using non-standardized frameworks, leading to incomparable results. Moreover, the introduction of extra learnable parameters on top of CLIP-style models compromises the reliability of the assessment. For example, while BiomedCLIP and PMC-CLIP show at least a 40% performance gap across all classification and retrieval tasks, this gap narrows to just 7% in Open-VQA, suggesting that (all things equal) the added decoders are capturing much of the information needed to solve the proposed tasks, as supposed to the evaluated encoder models.

As a way to evaluate our models and as an initial step in addressing these issues, we conduct a systematic assessment of zero-shot performance across 40 datasets, incorporating existing evaluations as thoroughly as possible, given data availability and reproducibility constraints. We include additional datasets to encompass previously overlooked biomedical domains. Lastly, all models are evaluated using the same framework, ensuring a fair and consistent comparison.

3. BIOMEDICA Data Curation Process

Our dataset curation workflow is illustrated in Figure 2, and consists of three stages: (1) dataset extraction, (2) concept labeling, and (3) dataset serialization.

Concept	Provenance
Image Data	
Image Key	Generated
Image File	File List
Caption	nXML File
Image Metadata	
Image Cluster ID	Generated
Image Hash	Generated
Image File Name	nXML File
Image Set	nXML File
Image Context	nXML File
Image Annotations	
Image Panel Type	Generated
Image Panel Subtype	Generated
Image Content Primary Label	Generated
Image Content Secondary Label	Generated
Article Metadata	
Article Keywords	nXML File
Article Category	nXML File
Article Title	nXML File
Article Abstract	nXML File
Article full text	nXML File
Article Publication Date	Entrez API
Article MeSH Terms	Entrez API
Article Journal	File List
Article PMID	File List
Article Citation	File List
Article License	File List
List of PMIDs citing article	Entrez API
Count of PMIDs citing article	Entrez API
Image Embeddings	
Image DINO-V2 Features	Generated
Image PMC-CLIP Features	Generated

Table 2. List of image data (n=3), image metadata (n=5), image annotations (n=4), article metadata (n=13), and image embeddings (n=2) provided in BIOMEDICA dataset, alongside concept provenance.

3.1. Data Extraction

Collected article data and metadata is stored in JSONL files. Table 2 lists all the extracted data along with its provenance.

Media file download Compressed files containing articles (stored as nXML files) and media files are downloaded from the National Center for Biotechnology Information (NCBI) via the File Transfer Protocol service⁴[41, 44] from July 2 to September 20, 2024.

Article retrieval Article data and metadata is aggregated from the retrieved file list, nXML files and the Entrez API.

- **File List:** Contains metadata fields to link articles to their corresponding media files. We iterate over this index, collecting PMID (accession ID), media file paths, publication date, references, journal and license.
- **nXML file:** Articles are provided in a structured nXML file. By parsing the nXML, we extract article data, including: title, abstract, keywords, category, full text, figure mentions and captions.
- **Entrez API:** The Entrez API provides access to NCBI’s full collection of biomedical literature metadata, allowing the retrieval of additional information. Through this API, we collect MeSH terms and PMIDs of citing articles.

⁴https://ftp.ncbi.nlm.nih.gov/pub/PMC/oa_package/

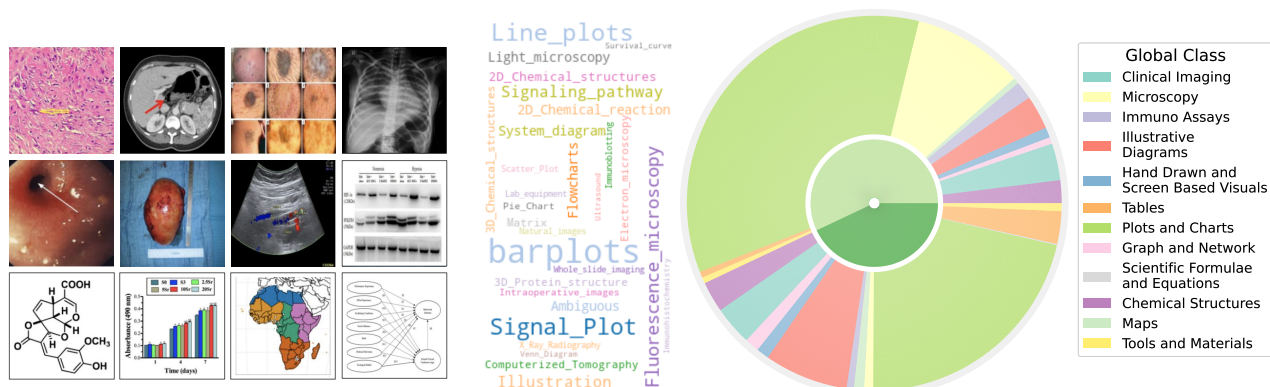


Figure 3. **Left:** Examples of images included in the BIOMEDICA dataset, ranging from clinical imaging to maps and bar plots. **Right:** Visualization of the concept breakdown in the BIOMEDICA taxonomy. The inner level of the pie chart reflects the *panel type* (light green indicates multi panel, dark green indicates single panel) and the outer level reflects the *global concept* of individual taxonomies, and the word cloud reflects the fine-grained *local concept* proportions for the most frequent concepts.

Figure Caption Each figure is matched with its corresponding caption by finding the graphic element in the nXML tree with an `@xlink:href` attribute matching the image id.

Figure Mentions In addition to the captions, we extract figure mentions—paragraphs in the article text that reference a given figure. To this end, we search for all XML tags with figure attribute `<xref ref-type="fig" ...>` and store all matched paragraphs. We leave the identifier tag within each paragraph to indicate the exact location where the figure is referenced.

License: Each image-caption pair entry includes the associated license information and the article citation. To the best of our knowledge, we adhere to all license terms provided by NCBI. To maintain strict compliance, we followed the three primary license groups—commercial, non-commercial, and other.

3.2. Concept Labeling

Feature Clustering All images are embedded using DINO-v2 [11] (ViT-L-14 distilled) and further reduced to 25 principal components (refer to Figure 7) using PCA. Subsequently, the compacted features are over-clustered using K-means with $K = 2000$.

Concept taxonomy A team of two licensed clinicians (pathology and surgery) and a bioinformatician were tasked with developing a hierarchical taxonomy for concepts within PMC-OA. First, an initial taxonomy is derived from biomedical ontologies including Uberon [40], NCBITaxon [17], and the Cell Line Ontology [48]. Subsequently, 30 samples are randomly sampled from each cluster. Annotators are then tasked to review the image content of these clusters to expand the taxonomy, refining it over three iterative rounds. The taxonomy is presented in figure 18.

Cluster Annotation A group of seven individuals with ex-

pertise in genetics, pathology, surgery, developmental biology, and biomedical informatics were tasked to annotate each cluster using the generated taxonomy. Using the majority of observations within a cluster, annotators were instructed to provide either one or multiple global and local concept labels, identify whether the images were multi-panel, and, if so, specify the types of sub-panels included (see Section 14).

Label Resolution and Propagation A majority voting system is employed to determine concept labels (see Section 14). In cases of ties, labels are re-evaluated. Once the final labels are assigned, a hash map linking cluster IDs to label metadata is used to propagate the annotations to individual images.

3.3. Data Serialization

Table 8 shows total compute time for parallelized data serialization. We convert the annotated paired media-JSON files into WebDataset format (following OpenClip’s naming convention for images and captions). This structure ensures that the dataset can be efficiently processed and distributed on demand via streaming, improving scalability.

Dataset Access To facilitate efficient user access, we make the BIOMEDICA dataset available on Hugging Face. This enables users to stream our large dataset directly from the Hub without downloading the entire artifact and provides seamless access even with limited local random access memory through memory mapping.

4. BIOMEDICA Dataset Description

Downloaded Articles A total of 6,042,494 articles are downloaded from the NCBI server through FTP. Within this collection, 5,050,473 articles have at least one image, while

992,021 articles are text-only. All articles have a corresponding nXML that contains the full text. Example images are shown in Figure 3.

Image-caption pairs collected From the full-text articles and associated image files, we collected a total of 24,076,288 unique image-caption pairs and extracted 30,711,542 figure references. On average, each article contains 4.9 images and each image is accompanied by 1.6 figure references.

Table 7 presents detailed text and image statistics. Caption token lengths range from a single token to 12,389 tokens, with a median length of 64 tokens, indicating that most captions are concise but can vary substantially. In contrast, figure reference paragraphs—which describe or contextualize images within the article—tend to be longer, with token counts reaching up to 699,117 tokens and a median of 338 tokens, showing the level of detail often required for clinical or scientific context. Overall, the text content includes a total of 2.84×10^9 tokens for captions, and 6.65×10^{10} tokens for the full text, illustrating the extensive scale of language data within the dataset.

For images, the median image width and height are 709 and 476 pixels, respectively. However, the wide range in both dimensions, from pixel up to tens of thousands (with a maximum width of 52,490 pixels and height of 65,081 pixels). This variability is due to the presence of both thumbnails or low-resolution images and high-resolution images, such as full-page figures or detailed illustrations.

Image taxonomy The image taxonomy comprises 12 global concepts and 170 local concepts as shown in Figure 3. A total of 23,271,916 images are covered by this taxonomy.

Table 16 shows image counts by global concept. Biomedical (microscopy and clinical imaging) images represent 17% of the total dataset. Notably, biomedical images are more common in noncommercial publications, where they make up 13% of the images, compared to 5% and 6% in commercial and other license categories, respectively. The “Plots and Charts” category holds the largest count across all source types, with a total of over 13 million images, which is 57% of the images, demonstrating that graphical data representations are common across scientific literature.

Each global concept is further divided into local concepts to capture the specific image types within broader categories. “Plots and Charts” has the most detailed taxonomy, with 96 local concepts, representing data visualizations like bar charts, line graphs, and heatmaps. “Clinical Imaging” follows with 34 local concepts, covering a range of imaging techniques including MRI, CT, and ultrasound.

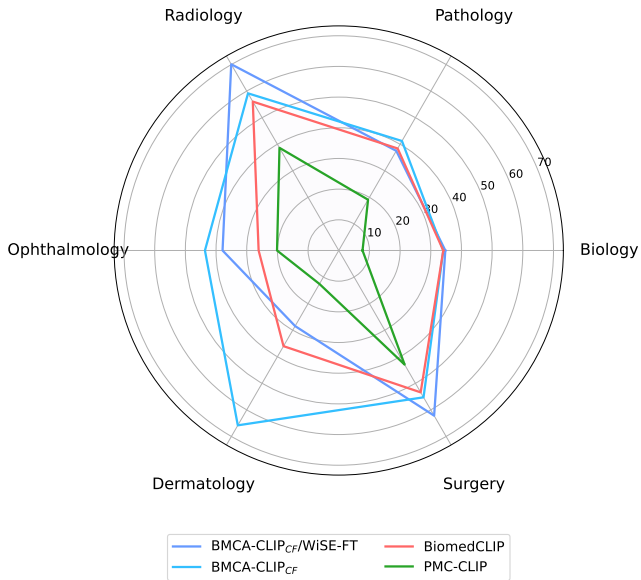


Figure 4. Average model performance of best BMCA-CLIP models compared to prior work.

5. Evaluation Benchmark

To evaluate the effectiveness of continual pretraining on the BIOMEDICA dataset, we repurposed 39 established biomedical classification tasks and leveraged a new retrieval dataset based on Flickr, for a total of 40 datasets.

Image classification To construct a comprehensive classification benchmark, we take the union of evaluations from prior work (BioMedCLIP and PMC-CLIP) and supplement it with underrepresented domains. For each individual task, classes are converted into captions (see Supplements), providing two variations per class. This evaluation set spans multiple fields: pathology (11 tasks), radiology (3 tasks), ophthalmology (1 task), dermatology (1 task), surgery (10 tasks), biology (9 tasks) and general microscopy (4 tasks). The biology and pathology tasks are sourced from Micro-Bench [38]; ophthalmology and dermatology tasks from MedMnist [63]; radiology tasks from RSNA [50] and CheXpert [26]; and minimal invasive (M.I.) surgery tasks are collected from the Dresden surgical anatomy dataset [12]. Table 12 provides a short description, citation, and domain.

The image classification benchmark is subdivided into two splits, similar to Micro-Bench [38]. The first category, general bioimaging classification, encompasses tasks such as diagnosis, object identification, and cellular profiling (e.g. determining cell state). This subset covers 35 tasks.

The second split, microscopy composition identification, is derived from the Micro-Bench Perception coarse-grained

Model	Biology		Pathology			Radiology		Ophthalmology	Dermatology	Surgery	Average
	Cell Profiling 6 (5)	Structure Profiling 3 (7)	Cytology 3 (6)	Neo-Histopath 4 (5)	Non Neo-Histopath 4 (3)	Chest X-ray 2 (3)	Breast ultrasound 1 (2)	Fundus Camera 1 (4)	Skin diagnosis 1 (7)	M.I. surgery 10* (2)	Total 35 (4)
Random	20.00	14.28	16.66	20.00	33.33	33.33	50.00	25.00	28.00	50.00	29.06
OpenCLIP [25]	24.63	44.84	<u>20.24</u>	43.88	36.81	60.88	<u>68.27</u>	23.75	20.37	<u>67.51</u>	41.18
CoCa [65]	23.58	32.92	36.27	36.50	38.33	24.69	30.45	43.50	10.15	36.78	31.12
PMC-CLIP [34]	6.01	11.23	12.48	29.86	7.82	28.47	58.97	20.12	12.59	42.96	23.05
BioMedCLIP [67]	<u>26.54</u>	49.14	17.03	48.83	42.39	56.04	56.09	26.12	36.01	53.40	41.16
BMCA-CLIP _{CF}	24.36	53.51	19.48	55.81	38.60	56.68	64.10	43.62	65.81	55.27	47.72
BMCA-CLIP _{CB}	23.54	50.35	16.39	<u>52.33</u>	33.62	50.34	66.35	<u>43.50</u>	<u>56.01</u>	56.51	44.89
BMCA-CLIP	23.56	48.66	16.61	51.97	34.55	53.06	56.41	43.00	23.07	62.64	41.35
BMCA-CLIP _{CF} /WiSE-FT	26.27	<u>51.68</u>	16.67	49.08	<u>39.07</u>	71.50	67.31	37.88	28.45	62.18	<u>45.01</u>
BMCA-CLIP _{CB} /WiSE-FT	24.66	50.44	17.19	49.09	38.50	64.59	70.19	36.75	24.06	62.39	43.79
BMCA-CLIP/WiSE-FT	27.70	47.67	16.82	44.19	38.62	<u>66.32</u>	<u>68.27</u>	27.62	15.84	67.68	42.07

Table 3. **General Biomedical Imaging Classification** Average zero-shot performance across 35 classification tasks (from 21 unique datasets) stratified by domain and task. We show results for three variants of our model, including continual pretraining on all of BIOMEDICA, a subset after concept-filtering (CF), and a subset after concept-balancing (CB). Models with indication WiSE-FT are merged counterparts as described in [59]. **Bold** indicates best performance, underline indicates second best performance.

benchmark. It spans both pathology and biology across light, fluorescence, and electron microscopy. These tasks involve identifying basic micrograph properties, including:

1. The domain (DM) or field of the image (e.g. pathology)
2. The microscopy modality (MD) and submodality (SM) used for image acquisition (e.g. light microscopy)
3. The staining technique (ST) applied to the specimen.

Retrieval task selection Since PMC-15M is not publicly available at the time of this manuscript, we cannot split BIOMEDICA dataset into the similar train and test sets as prior work while simultaneously ensuring a balanced number of concepts within each split. Therefore, we assess retrieval performance using a new collection of 7K high-quality, open-source biomedical image-caption pairs from Flickr. This benchmark spans concepts across pathology, radiology, biology, dermatology, and surgery (see Supplements Section 17 for a dataset description and samples).

Metrics. Classification tasks are evaluated using average accuracy across two caption variations, while retrieval tasks are measured using retrieval at 1, 10, and 100. Despite variations in the number of classes and samples across tasks, summary statistics are reported as unweighted averages, ensuring each task is treated with equal importance.

6. Experiments

We examine the effects of (1) continual pretraining on the full set of 24M image-caption pairs and compare these insights against (2) topic balancing, (3) dataset filtering, (4) robust fine-tuning. Additionally, we (5) include a baseline approach involving training a model from scratch using random weight initialization. This topic exploration is non-exhaustive and it is designed to utilize the supplementary annotations, metadata, and features made available in our dataset.

For all experiments, we use a batch size of 1024 per

GPU, distributed across four H100 80GB GPUs with a batch accumulation frequency of two steps, yielding an effective batch size of 8192 samples per step. We use a learning rate of 1e-6 with 1K warmup, and 32-bit floating-point precision. All of our experiments are trained via streaming, eliminating the need for local storage of the 27TB dataset. Additional training details are shared in supplements section 15. With these configurations, we run the following experiments:

1. **Continual pretraining on full dataset (24M)** In this experiment, we continually pretrain OpenCLIP (ViT-L-14) on the complete dataset of 24,076,288 pairs. We train each model for 9 epochs. This experiment serves as a baseline to compare additional data mixture strategies.
2. **Concept-Balancing (8M)** For this experiment, we continually pretrain a OpenCLIP (ViT-L-14) model on 8,404,992 pairs, balancing all topics for 27 epochs. To this end, over represented topics (e.g. plots) are dropped. This experiment targets potential biases introduced by data imbalance by restricting category over-representation.
3. **Concept-Filtering (6M)** In this experiment, we continually pretrain a OpenCLIP (ViT-L-14) using a filtered dataset of 6,602,752 image-caption pairs. This dataset includes only concepts within clinical and scientific imaging, immunoassays, illustrative diagrams, chemical structures, maps, tools and materials, and hand-drawn/screen-based visuals (excluding tables, figures, and scientific equations). We train the model for 36 epochs.
4. **Robust Fine-tuning** This experiment explores model merging [59] by using a convex combination of the weights from a base model and its adapted counterpart.

Model	Image → Text			Text → Image		
	Recall@1	Recall@10	Recall@100	Recall@1	Recall@10	Recall@100
OpenCLIP [25]	2.78	9.78	26.75	2.91	9.51	24.59
CoCa [65]	1.68	5.47	15.96	1.50	5.51	15.24
PMC-CLIP [34]	0.03	0.13	1.39	0.00	0.13	1.50
BiomedCLIP [67]	3.70	12.78	<u>36.27</u>	<u>3.94</u>	<u>13.63</u>	<u>35.63</u>
BMCA-CLIP _{CF}	4.13	15.13	38.30	4.15	13.75	36.10
BMCA-CLIP _{CB}	3.90	13.24	33.43	3.66	12.22	31.80
BMCA-CLIP	3.67	12.72	31.93	3.41	11.20	30.03
BMCA-CLIP _{CF} /WiSE-FT	<u>3.90</u>	13.24	33.43	3.66	12.22	31.80
BMCA-CLIP _{CB} /WiSE-FT	3.97	<u>13.57</u>	33.32	3.58	12.43	31.82
BMCA-CLIP/WiSE-FT	3.83	12.68	30.94	3.26	11.57	29.19

Table 4. Top-K retrieval performance on BioMed-Flickr. **Bold** indicates best performance, underline indicates second best performance.

Model	DM	MD	ST	SMD	Avg.
OpenCLIP [25]	49.67	85.66	46.77	<u>29.23</u>	53.03
CoCa [65]	47.29	71.89	39.27	48.00	47.29
PMC-CLIP [34]	5.56	14.68	10.92	12.49	10.91
BioMedCLIP [67]	41.54	74.72	49.74	32.89	49.72
BMCA-CLIP _{CF}	49.07	78.71	59.17	14.54	50.37
BMCA-CLIP _{CB}	40.07	83.4	57.28	25.48	51.55
BMCA-CLIP	44.56	85.70	58.40	26.72	53.84
BMCA-CLIP _{CF} /WiSE-FT	58.78	<u>86.88</u>	<u>60.84</u>	27.65	58.53
BMCA-CLIP _{CB} /WiSE-FT	52.12	87.21	61.84	25.04	<u>56.55</u>
BMCA-CLIP/WiSE-FT	<u>56.26</u>	83.97	54.81	27.89	55.73

Table 5. **Microscopy Composition Identification** Performance in 4 course-grained classification tasks from μ -Bench Perception across pathology and biology. **Bold** indicates best performance, underline indicates second best performance.

7. Results

Concept Filtering leads to better performance across zero-shot classification and retrieval tasks Intuitively, when compared to other continual pretraining strategies within BMCA-CLIP models, filtering the dataset (e.g., dropping over-represented topics like plots and tables) yields the best average performance across general biomedical imaging classification tasks with respect to concept balancing (better 80% of the time) and full-dataset pretraining (better 90% of the time). Additionally, concept filtering leads to superior performance compared to concept balancing or full-dataset pretraining in image-to-text and text-to-image retrieval. Indeed, within this training strategy, 48% of the data mixture corresponds to clinical imaging and microscopy.

Models Trained on the BIOMEDICA Dataset Lead to State-of-the-Art Zero-Shot Performance Compared to prior work, models trained on the BIOMEDICA dataset yield better average performance in classification and retrieval tasks. BMCA-CLIP_{CF} outperforms PMC-CLIP

in all tasks, achieving a +24.67% improvement in general biomedical imaging classification tasks, with a minimum gap of +5.13% in ultrasound (radiology) and a maximum gap of +53.22% in dermatology. Similarly, a +39.46% improvement is observed in microscopy composition tasks. Additionally, a recall@100 gap of +36.91% and +34.6% is observed in image-to-text and text-to-image retrieval, respectively. Similarly, BMCA-CLIP_{CF} outperforms BioMedCLIP in 8/10 general biomedical imaging classification subsets, yielding an average improvement of 6.56%. For individual tasks, BMCA-CLIP_{CF} achieves the highest differential performance w.r.t BioMedCLIP in dermatology (+29.8%), ophthalmology (+17.5%), breast ultrasound (+8.01%) and non-neo histopathology (+6.98%) and marginal better performance in microscopy composition identification and all retrieval evaluations. It is noteworthy to highlight that BMCA-CLIP_{CF} achieves these results while using 10× less compute and 2.5× less data.

Robust Fine-tuning complements model performance in a subset of tasks Another advantage of our setup (continual pretraining) is its capability to improve individual task performance without further training, as shown in previous work [38, 59]. For example, in microscopy composition identification tasks, WiSE-FT improves BMCA-CLIP_{CF} by 8.16%, further increasing the performance gap with respect to BioMedCLIP. Similarly, WiSE-FT enhances BMCA-CLIP_{CF}'s performance in 5/10 general biomedical imaging classification tasks (see Figure 4). Notably, BMCA-CLIP_{CF}/WiSE-FT increases the performance gap w.r.t BioMedCLIP in X-ray radiology (+15.46%), breast ultrasound (+11.22%), and surgery (+8.78%), complementing weakness in the original BMCA-CLIP_{CF} model. However, this gain in performance comes at the cost of lower performance in other subtasks, such as -7.56% in dermatology and marginally worse retrieval performance.

8. Limitations

While our models offer state-of-the-art performance, all evaluations indicate that there is still significant room for improvement. We highlight two promising directions:

Short context length: CLIP (ViT-L-14) has a maximum context length of 77 tokens, which restricts our ability to fully utilize captions exceeding this length. While the median caption length in our dataset is 64 tokens, there remains a portion of longer captions that cannot be leveraged in their entirety during continual pre-training. This limitation may lead to information loss potentially impacting model performance on tasks requiring more comprehensive textual understanding.

Varied image size: The BIOMEDICA dataset contains images of diverse sizes and resolutions, reflective of the original formats in the PMC Open Access Subset. For model training, all images are uniformly resized to meet the input requirements of the image encoder, without any preprocessing to address the variation in image quality or aspect ratios. High-resolution images with fine-grained details may lose important visual information when downscaled, while low-resolution images may become blurry when upscaled, distorting features and potentially introducing misleading information.

9. Conclusion

In this work, we present BIOMEDICA, a framework for converting PMC-OA into the largest deep-learning-ready dataset, comprising 24 million image-caption pairs with 27 metadata fields derived from scientific literature. We demonstrate the utility of the BIOMEDICA dataset by continually pretraining CLIP-style models, fully leveraging its expert-guided annotations, metadata, and streaming capabilities. Our results showcase the effectiveness of this resource, even in low-memory and GPU-constrained scenarios.

Our models achieve state-of-the-art zero-shot classification performance using prior open-source tools and models, while utilizing 10x less compute and 2.5x less data—underscoring the importance of large-scale annotated open datasets. The BIOMEDICA framework, dataset, models, and large-scale evaluation serve as a foundation for advancing vision-language research and applications in scientific and biomedical domains. We release all our contributions under a permissive license to facilitate broader use and further development.

9.1. Acknowledgments

This research was supported by NIH grants (NIH#P30AG066515 to JJN), the Chan Zuckerberg

Initiative Neurodegeneration Challenge Pairs Pilot Project to SYL (2020-221724, 5022), the Wu Tsai Knight Initiative Innovation grant (#KIG 102) to SYL, Hoffman-Yee Research Grant to SYL, the Arc Institute Graduate Fellowship to AL, the Stanford Data Science Graduate Research Fellowship MW, and the Quad Fellowship to JB, and. SYL is a Chan Zuckerberg Biohub – San Francisco Investigator. We also thank Daniel van Strien, Matthew Carrigan, and Omar Sanseviero from Hugging Face for their invaluable assistance with data upload and design planning on the Hugging Face platform.

References

- [1] Andrea Acevedo, Anna Merino, Santiago Alférez, Ángel Molina, Laura Boldú, and José Rodellar. A dataset of microscopic peripheral blood cell images for development of automatic recognition systems. *Data Brief*, 30(105474):105474, 2020. 8
- [2] Titipat Achakulvisut, Daniel E Acuna, and Konrad Kording. Pubmed parser: A python parser for pubmed open-access xml subset and medline xml dataset xml dataset. *Journal of Open Source Software*, 5(46):1979, 2020. 4
- [3] Josh Achiam, Steven Adler, Sandhini Agarwal, Lama Ahmad, Ilge Akkaya, Florencia Leoni Aleman, Diogo Almeida, Janko Altenschmidt, Sam Altman, Shyamal Anadkat, et al. Gpt-4 technical report. *arXiv preprint arXiv:2303.08774*, 2023. 2
- [4] Walid Al-Dhabyani, Mohammed Gomaa, Hussien Khaled, and Aly Fahmy. Dataset of breast ultrasound images. *Data in brief*, 28:104863, 2020. 8
- [5] Ibrahim Alabdulmohsin, Xiao Wang, Andreas Steiner, Priya Goyal, Alexander D’Amour, and Xiaohua Zhai. Clip the bias: How useful is balancing data in multimodal learning? *arXiv preprint arXiv:2403.04547*, 2024. 4
- [6] Sebastiano Battiato, Alessandro Ortis, Francesca Trenta, Lorenzo Ascari, Mara Politi, and Consolata Siniscalco. Pollen13k: A large scale microscope pollen grain image dataset. *2020 IEEE International Conference on Image Processing (ICIP)*, pages 2456–2460, 2020. 8
- [7] Leif Bertilsson, Marja-Liisa Dahl, Per Dalén, and Ayman Al-Shurbaji. Molecular genetics of cyp2d6: clinical relevance with focus on psychotropic drugs. *British journal of clinical pharmacology*, 53(2):111–122, 2002. 3
- [8] AA Borkowski, MM Bui, LB Thomas, CP Wilson, LA DeLand, and SM Mastorides. Lung and colon cancer histopathological image dataset (lc25000). arxiv 2019. *arXiv preprint arXiv:1912.12142*. 8
- [9] Andrew A Borkowski, Marilyn M Bui, L Brannon Thomas, Catherine P Wilson, Lauren A DeLand, and Stephen M Mastorides. Lung and colon cancer histopathological image dataset (lc25000). *arXiv preprint arXiv:1912.12142*, 2019. 5
- [10] James Burgess, Jeffrey J Nirschl, Maria-Clara Zanellati, Alejandro Lozano, Sarah Cohen, and Serena Yeung-Levy. Orientation-invariant autoencoders learn robust representa-

- tions for shape profiling of cells and organelles. *Nat. Commun.*, 15(1), 2024. 8
- [11] Mathilde Caron, Hugo Touvron, Ishan Misra, Hervé Jégou, Julien Mairal, Piotr Bojanowski, and Armand Joulin. Emerging properties in self-supervised vision transformers. In *Proceedings of the IEEE/CVF international conference on computer vision*, pages 9650–9660, 2021. 6
- [12] Matthias Carstens, Franziska M Rinner, Sebastian Bodenstedt, Alexander C Jenke, Jürgen Weitz, Marius Distler, Stefanie Speidel, and Fiona R Kolbinger. The dresden surgical anatomy dataset for abdominal organ segmentation in surgical data science. *Scientific Data*, 10(1):1–8, 2023. 7, 8
- [13] Mehdi Cherti, Romain Beaumont, Ross Wightman, Mitchell Wortsman, Gabriel Ilharco, Cade Gordon, Christoph Schuhmann, Ludwig Schmidt, and Jenia Jitsev. Reproducible scaling laws for contrastive language-image learning. In *Proceedings of the IEEE/CVF Conference on Computer Vision and Pattern Recognition*, pages 2818–2829, 2023. 4
- [14] Azra Daei, Mohammad Reza Soleymani, Hasan Ashrafi-Rizi, Ali Zargham-Boroujeni, and Roya Kelishadi. Clinical information seeking behavior of physicians: A systematic review. *International journal of medical informatics*, 139: 104144, 2020. 2
- [15] Guilherme Del Fiore, T Elizabeth Workman, and Paul N Gorman. Clinical questions raised by clinicians at the point of care: a systematic review. *JAMA internal medicine*, 174(5): 710–718, 2014. 2
- [16] Karan Desai, Gaurav Kaul, Zubin Aysola, and Justin Johnson. Redcaps: Web-curated image-text data created by the people, for the people. *arXiv preprint arXiv:2111.11431*, 2021. 2
- [17] Rezarta Islamaj Doğan, Robert Leaman, and Zhiyong Lu. Ncbi disease corpus: a resource for disease name recognition and concept normalization. *Journal of biomedical informatics*, 47:1–10, 2014. 6
- [18] Sedigheh Eslami, Christoph Meinel, and Gerard De Melo. Pubmedclip: How much does clip benefit visual question answering in the medical domain? In *Findings of the Association for Computational Linguistics: EACL 2023*, pages 1181–1193, 2023. 4
- [19] Philipp Eulenberger, Niklas Köhler, Thomas Blasi, Andrew Filby, Anne E Carpenter, Paul Rees, Fabian J Theis, and F Alexander Wolf. Reconstructing cell cycle and disease progression using deep learning. *Nature communications*, 8(1): 463, 2017. 8
- [20] Alex Fang, Albin Madappally Jose, Amit Jain, Ludwig Schmidt, Alexander Toshev, and Vaishal Shankar. Data filtering networks. *arXiv preprint arXiv:2309.17425*, 2023. 4
- [21] Scott L Fleming, Alejandro Lozano, William J Haberkorn, Jenelle A Jindal, Eduardo Reis, Rahul Thapa, Louis Blankemeier, Julian Z Jenkins, Ethan Steinberg, Ashwin Nayak, et al. Medalign: A clinician-generated dataset for instruction following with electronic medical records. In *Proceedings of the AAAI Conference on Artificial Intelligence*, pages 22021–22030, 2024. 2
- [22] Rita González-Márquez, Luca Schmidt, Benjamin M Schmidt, Philipp Berens, and Dmitry Kobak. The landscape of biomedical research. *Patterns*, 2024. 2
- [23] Zepeng Huo, Jason Alan Fries, Alejandro Lozano, Jeya Maria Jose Valanarasu, Ethan Steinberg, Louis Blankemeier, Akshay S Chaudhari, Curtis Langlotz, and Nigam H Shah. Time-to-event pretraining for 3d medical imaging. *arXiv preprint arXiv:2411.09361*, 2024. 2
- [24] Elima Hussain, Lipi B Mahanta, Himakshi Borah, and Chandana Ray Das. Liquid based-cytology pap smear dataset for automated multi-class diagnosis of pre-cancerous and cervical cancer lesions. *Data Brief*, 30(105589):105589, 2020. 8
- [25] Gabriel Ilharco, Mitchell Wortsman, Ross Wightman, Cade Gordon, Nicholas Carlini, Rohan Taori, Achal Dave, Vaishal Shankar, Hongseok Namkoong, John Miller, Han-naneh Hajishirzi, Ali Farhadi, and Ludwig Schmidt. Openclip, 2021. If you use this software, please cite it as below. 8, 9
- [26] Jeremy Irvin, Pranav Rajpurkar, Michael Ko, Yifan Yu, Silvana Ciurea-Ilcus, Chris Chute, Henrik Marklund, Behzad Haghgoo, Robyn Ball, Katie Shpanskaya, Jayne Seekins, David A. Mong, Safwan S. Halabi, Jesse K. Sandberg, Ricky Jones, David B. Larson, Curtis P. Langlotz, Bhavik N. Patel, Matthew P. Lungren, and Andrew Y. Ng. Chexpert: A large chest radiograph dataset with uncertainty labels and expert comparison, 2019. 7
- [27] Jeremy Irvin, Pranav Rajpurkar, Michael Ko, Yifan Yu, Silvana Ciurea-Ilcus, Chris Chute, Henrik Marklund, Behzad Haghgoo, Robyn Ball, Katie Shpanskaya, et al. Chexpert: A large chest radiograph dataset with uncertainty labels and expert comparison. In *Proceedings of the AAAI conference on artificial intelligence*, pages 590–597, 2019. 8
- [28] Andrii Iudin, Paul K Korir, Sriram Somasundharam, Simone Weyand, Cesare Cattavittello, Neli Fonseca, Osman Salih, Gerard J Kleywegt, and Ardan Patwardhan. Empiar: the electron microscopy public image archive. *Nucleic Acids Research*, 51(D1):D1503–D1511, 2023. 8
- [29] Qiao Jin, Zifeng Wang, Charalampos S Floudas, Fangyuan Chen, Changlin Gong, Dara Bracken-Clarke, Elisabetta Xue, Yifan Yang, Jimeng Sun, and Zhiyong Lu. Matching patients to clinical trials with large language models. *Nature Communications*, 15(1):9074, 2024. 2
- [30] KV Jobin, Ajoy Mondal, and CV Jawahar. Docfigure: A dataset for scientific document figure classification. In *2019 International Conference on Document Analysis and Recognition Workshops (ICDARW)*, pages 74–79. IEEE, 2019. 4
- [31] Changhun Jung, Mohammed Abuhamad, David Mohaisen, Kyungja Han, and DaeHun Nyang. Wbc image classification and generative models based on convolutional neural network. *BMC Medical Imaging*, 22(1):94, 2022. 8
- [32] Jakob Nikolas Kather, Cleo-Aron Weis, Francesco Bianconi, Susanne M Melchers, Lothar R Schad, Timo Gaiser, Alexander Marx, and Frank Gerrit Zöllner. Multi-class texture analysis in colorectal cancer histology. *Sci. Rep.*, 6:27988, 2016. 8
- [33] Zichao Li, Cihang Xie, and Ekin Dogus Cubuk. Scaling (down) clip: A comprehensive analysis of data, architecture, and training strategies. *arXiv preprint arXiv:2404.08197*, 2024. 4

- [34] Weixiong Lin, Ziheng Zhao, Xiaoman Zhang, Chaoyi Wu, Ya Zhang, Yanfeng Wang, and Weidi Xie. Pmc-clip: Contrastive language-image pre-training using biomedical documents. In *International Conference on Medical Image Computing and Computer-Assisted Intervention*, pages 525–536. Springer, 2023. 3, 4, 8, 9
- [35] Geert Litjens, Peter Bandi, Babak Ehteshami Bejnordi, Oscar Geessink, Maschenka Balkenhol, Peter Bult, Altuna Halilovic, Meyke Hermesen, Rob Van de Loo, Rob Vogels, et al. 1399 h&e-stained sentinel lymph node sections of breast cancer patients: the camelyon dataset. *GigaScience*, 7(6):giy065, 2018. 8
- [36] Ruhan Liu, Xiangning Wang, Qiang Wu, Ling Dai, Xi Fang, Tao Yan, Jaemin Son, Shiqi Tang, Jiang Li, Zijian Gao, et al. Deepdrid: Diabetic retinopathy—grading and image quality estimation challenge. *Patterns*, 3(6), 2022. 8
- [37] Alejandro Lozano, Scott L Fleming, Chia-Chun Chiang, and Nigam Shah. Clinfo. ai: An open-source retrieval-augmented large language model system for answering medical questions using scientific literature. In *PACIFIC SYMPOSIUM ON BIOC COMPUTING 2024*, pages 8–23. World Scientific, 2023. 2
- [38] Alejandro Lozano, Jeffrey Nirschl, James Burgess, Sanket Rajan Gupte, Yuhui Zhang, Alyssa Unell, and Serena Yeung-Levy. $\{\mu\}$ -bench: A vision-language benchmark for microscopy understanding. *arXiv preprint arXiv:2407.01791*, 2024. 3, 7, 9, 8
- [39] Michael Moor, Oishi Banerjee, Zahra Shakeri Hossein Abad, Harlan M Krumholz, Jure Leskovec, Eric J Topol, and Pranav Rajpurkar. Foundation models for generalist medical artificial intelligence. *Nature*, 616(7956):259–265, 2023. 2
- [40] Christopher J Mungall, Carlo Torniai, Georgios V Gkoutos, Suzanna E Lewis, and Melissa A Haendel. Uberon, an integrative multi-species anatomy ontology. *Genome biology*, 13:1–20, 2012. 6
- [41] National Library of Medicine. PMC Open Access Subset [Internet], 2003. Bethesda (MD): National Library of Medicine. [cited 2024 Jul 2]. Available from: <https://www.ncbi.nlm.nih.gov/pmc/tools/openftlist/>. 5
- [42] Jeffrey J Nirschl, Andrew Janowczyk, Eliot G Peyster, Renee Frank, Kenneth B Margulies, Michael D Feldman, and Anant Madabhushi. A deep-learning classifier identifies patients with clinical heart failure using whole-slide images of h&e tissue. *PLoS One*, 13(4):e0192726, 2018. 8
- [43] Obioma Pelka, Sven Koitka, Johannes Rückert, Felix Nensa, and Christoph M Friedrich. Radiology objects in context (roco): a multimodal image dataset. In *Intravascular Imaging and Computer Assisted Stenting and Large-Scale Annotation of Biomedical Data and Expert Label Synthesis: 7th Joint International Workshop, CVII-STENT 2018 and Third International Workshop, LABELS 2018, Held in Conjunction with MICCAI 2018, Granada, Spain, September 16, 2018, Proceedings 3*, pages 180–189. Springer, 2018. 3, 4, 5
- [44] Jon Postel and Joyce Reynolds. File transfer protocol. Technical report, 1985. 5
- [45] Alec Radford, Jong Wook Kim, Chris Hallacy, Aditya Ramesh, Gabriel Goh, Sandhini Agarwal, Girish Sastry, Amanda Askell, Pamela Mishkin, Jack Clark, et al. Learning transferable visual models from natural language supervision. In *International conference on machine learning*, pages 8748–8763. PMLR, 2021. 4
- [46] Richard J Roberts. Pubmed central: The genbank of the published literature, 2001. 2, 4
- [47] Khaled Saab, Tao Tu, Wei-Hung Weng, Ryutaro Tanno, David Stutz, Ellery Wulczyn, Fan Zhang, Tim Strother, Chunjong Park, Elahe Vedadi, et al. Capabilities of gemini models in medicine. *arXiv preprint arXiv:2404.18416*, 2024. 2
- [48] Sirarat Sarntivijai, Yu Lin, Zuoshuang Xiang, Terrence F Meehan, Alexander D Diehl, Uma D Vempati, Stephan C Schürer, Chao Pang, James Malone, Helen Parkinson, et al. Clo: the cell line ontology. *Journal of biomedical semantics*, 5:1–10, 2014. 6
- [49] Christoph Schuhmann, Romain Beaumont, Richard Vencu, Cade Gordon, Ross Wightman, Mehdi Cherti, Theo Coombes, Aarush Katta, Clayton Mullis, Mitchell Wortsman, et al. Laion-5b: An open large-scale dataset for training next generation image-text models. *Advances in Neural Information Processing Systems*, 35:25278–25294, 2022. 2, 4
- [50] George Shih, Carol C Wu, Safwan S Halabi, Marc D Kohli, Luciano M Prevedello, Tessa S Cook, Arjun Sharma, Judith K Amorosa, Veronica Arteaga, Maya Galperin-Aizenberg, et al. Augmenting the national institutes of health chest radiograph dataset with expert annotations of possible pneumonia. *Radiology: Artificial Intelligence*, 1(1):e180041, 2019. 5, 7
- [51] Sanjay Subramanian, Lucy Lu Wang, Sachin Mehta, Ben Bogin, Madeleine van Zuylen, Sravanthi Parasa, Sameer Singh, Matt Gardner, and Hannaneh Hajishirzi. Medcat: A dataset of medical images, captions, and textual references. *arXiv preprint arXiv:2010.06000*, 2020. 3, 4
- [52] Ziqi Tang, Kangway V Chuang, Charles DeCarli, Lee-Way Jin, Laurel Beckett, Michael J Keiser, and Brittany N Dugger. Interpretable classification of alzheimer’s disease pathologies with a convolutional neural network pipeline. *Nat. Commun.*, 10(1):2173, 2019. 8
- [53] Hugo Touvron, Thibaut Lavril, Gautier Izacard, Xavier Martinet, Marie-Anne Lachaux, Timothée Lacroix, Baptiste Rozière, Naman Goyal, Eric Hambro, Faisal Azhar, et al. Llama: Open and efficient foundation language models. *arXiv preprint arXiv:2302.13971*, 2023. 2
- [54] Philipp Tschandl. The HAM10000 dataset, a large collection of multi-source dermatoscopic images of common pigmented skin lesions, 2018. 8
- [55] Bastiaan S Veeling, Jasper Linmans, Jim Winkens, Taco Cohen, and Max Welling. Rotation equivariant CNNs for digital pathology. 2018. 5
- [56] Deepak Vohra and Deepak Vohra. Apache parquet. *Practical Hadoop Ecosystem: A Definitive Guide to Hadoop-Related Frameworks and Tools*, pages 325–335, 2016. 3
- [57] Daniel R Wong, Ziqi Tang, Nicholas C Mew, Sakshi Das, Justin Athey, Kirsty E McAleese, Julia K Kofler, Margaret E

- Flanagan, Ewa Borys, Charles L White, 3rd, Atul J Butte, Brittany N Dugger, and Michael J Keiser. Deep learning from multiple experts improves identification of amyloid neuropathologies. *Acta Neuropathol. Commun.*, 10(1):66, 2022. [8](#)
- [58] Michael Wornow, Alejandro Lozano, Dev Dash, Jenelle Jindal, Kenneth W Mahaffey, and Nigam H Shah. Zero-shot clinical trial patient matching with llms. *arXiv preprint arXiv:2402.05125*, 2024. [2](#)
- [59] Mitchell Wortsman, Gabriel Ilharco, Jong Wook Kim, Mike Li, Simon Kornblith, Rebecca Roelofs, Raphael Gontijo Lopes, Hannaneh Hajishirzi, Ali Farhadi, Hongseok Namkoong, et al. Robust fine-tuning of zero-shot models. In *Proceedings of the IEEE/CVF conference on computer vision and pattern recognition*, pages 7959–7971, 2022. [4](#), [8](#), [9](#)
- [60] Gong-Her Wu, Charlene Smith-Geater, Jesús G Galaz-Montoya, Yingli Gu, Sanket R Gupte, Ranen Aviner, Patrick G Mitchell, Joy Hsu, Ricardo Miramontes, Keona Q Wang, Nicolette R Geller, Cathy Hou, Cristina Danita, Lydia-Marie Joubert, Michael F Schmid, Serena Yeung, Judith Frydman, William Mobley, Chengbiao Wu, Leslie M Thompson, and Wah Chiu. CryoET reveals organelle phenotypes in huntington disease patient iPSC-derived and mouse primary neurons. *Nat. Commun.*, 14(1):692, 2023. [8](#)
- [61] Yan Yan, Rómer Rosales, Glenn Fung, Ramanathan Subramanian, and Jennifer Dy. Learning from multiple annotators with varying expertise. *Machine learning*, 95:291–327, 2014. [2](#)
- [62] An Yang, Baosong Yang, Binyuan Hui, Bo Zheng, Bowen Yu, Chang Zhou, Chengpeng Li, Chengyuan Li, Dayiheng Liu, Fei Huang, et al. Qwen2 technical report. *arXiv preprint arXiv:2407.10671*, 2024. [2](#)
- [63] Jiancheng Yang, Rui Shi, Donglai Wei, Zequan Liu, Lin Zhao, Bilian Ke, Hanspeter Pfister, and Bingbing Ni. Medmnist v2 - a large-scale lightweight benchmark for 2d and 3d biomedical image classification. *Scientific Data*, 10(1):41, 2023. [7](#)
- [64] Jiancheng Yang, Rui Shi, Donglai Wei, Zequan Liu, Lin Zhao, Bilian Ke, Hanspeter Pfister, and Bingbing Ni. Medmnist v2-a large-scale lightweight benchmark for 2d and 3d biomedical image classification. *Scientific Data*, 10(1):41, 2023. [5](#)
- [65] Jiahui Yu, Zirui Wang, Vijay Vasudevan, Legg Yeung, Mojtaba Seyedhosseini, and Yonghui Wu. Coca: Contrastive captioners are image-text foundation models. *arXiv preprint arXiv:2205.01917*, 2022. [8](#), [9](#)
- [66] Xiaohua Zhai, Basil Mustafa, Alexander Kolesnikov, and Lucas Beyer. Sigmoid loss for language image pre-training. In *Proceedings of the IEEE/CVF International Conference on Computer Vision*, pages 11975–11986, 2023. [4](#)
- [67] Sheng Zhang, Yanbo Xu, Naoto Usuyama, Hanwen Xu, Jaspreet Bagga, Robert Tinn, Sam Preston, Rajesh Rao, Mu Wei, Naveen Valluri, et al. Biomedclip: a multimodal biomedical foundation model pretrained from fifteen million scientific image-text pairs. *arXiv preprint arXiv:2303.00915*, 2023. [4](#), [8](#), [9](#)



BIOMEDICA: An Open Biomedical Image-Caption Archive, Dataset, and Vision-Language Models Derived from Scientific Literature

Supplementary Material

10. Supplementary Material Table of Content

1. Dataset Description
 - Dataset Statistics
 - Cohort Diagram
 - Entrez Statistics
2. Dataset Statistics
 - Context length
3. Dataset Curation Process
 - PMC OA Subset Description
 - Serialization at the Image-caption Level
4. Labeling
 - Dimensionality Reduction
 - Over Clustering
 - Taxonomy
 - Annotation Form
 - Correlation Analysis
 - Cluster Examples
5. Model Training Configuration
 - Base Model selection
 - Hyperparameters
6. Evaluation
 - Classification to VQA Conversion
 - Conversion Prompts
 - Evaluation Examples
 - Dataset Provenance Table.
 - Task Explanation
 - Performance by Dataset.
 - Bio-med Flicker and Statistics
 - Evaluate Retrieval Performance by Caption Length.
7. Compute Environment

Table 6. BIOMEDICA dataset statistics: Counts of articles, image-caption pairs, metadata, human annotators and specialties.

Aspect	Count
Articles	6,042,494
Articles with Images	5,050,473
Images	24,076,288
Captions	24,076,288
Figure Reference	30,711,542
Metadata	22
Global Concepts	13
Local Concepts	170
Clinical Annotators	2
Scientist Annotators	6

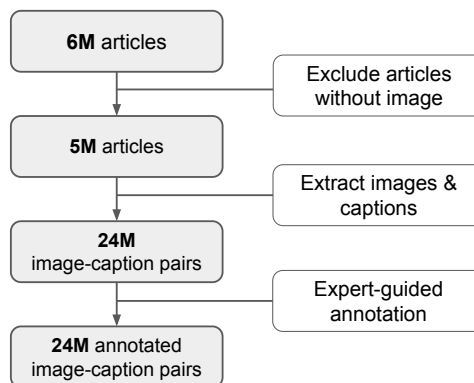


Figure 5. BIOMEDICA cohort diagram: selection criteria for the construction of relevant image-caption pairs.

11. Dataset Description

BIOMEDICA dataset contains a total of 24,076,288 image-caption pairs from 5,050,473 scientific articles. Each image-caption pairs is assigned article metadata and additional annotations. Table 6 shows descriptive statistics for BIOMEDICA dataset. Table 19 shows example image-caption pairs.

Figure 5 shows a cohort diagram, summarizing the materialization of BIOMEDICA dataset.

12. Dataset Statistics

We provide additional statistics for our dataset. The reference count, representing the number of articles citing a

given article, ranges from 0 to 3346, with a median of 37 (IQR: 35). Articles with no references account for 120,870 entries. A total of 263,836,608 references is found across the entire dataset.

For MeSH terms, the dataset includes 29,859 unique terms. MeSH term counts per article range from 0 to 44, with a median of 0 (IQR: 10) and a total of 32,896,861 terms. Notably, 2,991,141 articles are annotated with MeSH terms, emphasizing the dataset’s depth in biomedical categorization.

Table 14 summarizes the top 50 most frequent MeSH terms in the dataset.

Text Statistics	Min	Max	Median	IQR	Total
Caption Token Length	1	12389	64	134	2.84×10^9
Caption Character Length	1	25539	246	498	1.05×10^{10}
Figure Reference Token Length	17	699117	338	299	1.28×10^{10}
Figure Reference Character Length	39	1395195	1323	1162	4.82×10^{10}
Full Text Token Length	20	2449711	10306	8831	6.65×10^{10}
Full Text Character Length	70	8701762	39072	32080	2.47×10^{11}
Image Statistics					
Image Width (pixels)	1	52490	709	150	-
Image Height (pixels)	1	65081	476	406	-
Image Area (pixels ²)	1	1.95×10^9	334400	307272	-

Table 7. Overview of dataset statistics, detailing text token and character lengths, and image dimensions. For text statistics, tokens are generated using the BPE tokenizer from the `tiktoken` library

13. Data Curation Process

Besides releasing the code to make BIOMEDICA dataset fully reproducible, we provide additional descriptions and design choices for the dataset curation process. To increase efficiency and enable scaling, everything step in the data curation process is parallelized, unless specified otherwise.

13.1. PMC OA Dataset Description

The PubMed Central (PMC) Open Access (OA) Subset is a publicly accessible collection of full-text scholarly articles hosted by the National Center for Biotechnology Information (NCBI). This subset contains articles that have been made available under various open-access licenses. It covers a wide range of disciplines within biomedical and life sciences, providing rich content that includes research articles, reviews, case reports, and clinical trials. As of 2024, over six million articles are available, with tens of thousands of new articles added annually, reflecting the continuous contributions of researchers worldwide.

13.2. Data Extraction

The remote paths to the compressed files (`tar.gz`) containing each article’s media files are listed in a CSV file, referred to as the file list. The file list provides the structure for locating and accessing the content, ensuring that all relevant files can be traced and downloaded accurately. The file list includes the following columns: *File*, *Citation*, *Accession_ID*, *Date*, *PMID*, and *License*. The server stores files with randomized paths to optimize storage; therefore, the absolute file path provided in the file list is required to retrieve the media files for a specific article. We connect to the server using the Python package `ftplib`:

```
ftp = FTP("ftp.ncbi.nlm.nih.gov")
ftp.retrbinary("RETR <remote_file_path>",
open("<local_file_path>", "wb").write)
```

Bulk downloads are available only for text files, necessitating individual retrieval of associated media files.

The server enforces a rate limit of three requests per second per IP address, with varying download speeds requiring precise scheduling to prevent disruptions. FTP connections may disconnect intermittently, requiring a robust retry mechanism with short delays to maintain data integrity. To conserve storage, only necessary files (`nxml` and `jpg`) are kept, while other files (e.g., `pdf`, `docx`, `xlsx`, `mp4`) are discarded if present.

After downloading and uncompressing all files, we create JSON files to store data extracted from the raw `nxml` and image files. These JSON files contain a list of dictionaries, where each dictionary holds the data for a single unique article. The `figure_set` is a list of dictionaries, where each dictionary contains the figure’s `PMID`, volume number, image file, caption, and context. This structure is shown in Figure 6.

Entrez is a search and retrieval system from NCBI that we use to collect additional metadata, including publication details and MeSH terms, which are not available in the file list or raw `nxml` files. The Entrez API supports batch queries with up to 200 PMIDs per request:

```
from Bio import Entrez
Entrez.email = "<your_email>"
handle = Entrez.efetch(
    db = "pubmed",
    id = "<comma_separated_PMIDs>",
    retmode = "xml")
```

Each JSON file is limited to a maximum of 200 articles to comply with the Entrez API batch limit and to keep file sizes manageable for processing.

13.3. Dataset Serialization

As shown in Figure 6 A, the retrieved data is a collection of articles with full metadata and a figure set (containing multiple images and captions). This structure can natively be serialized by article; however, it requires an extra iteration within the figure set. Instead, we decide to serialize

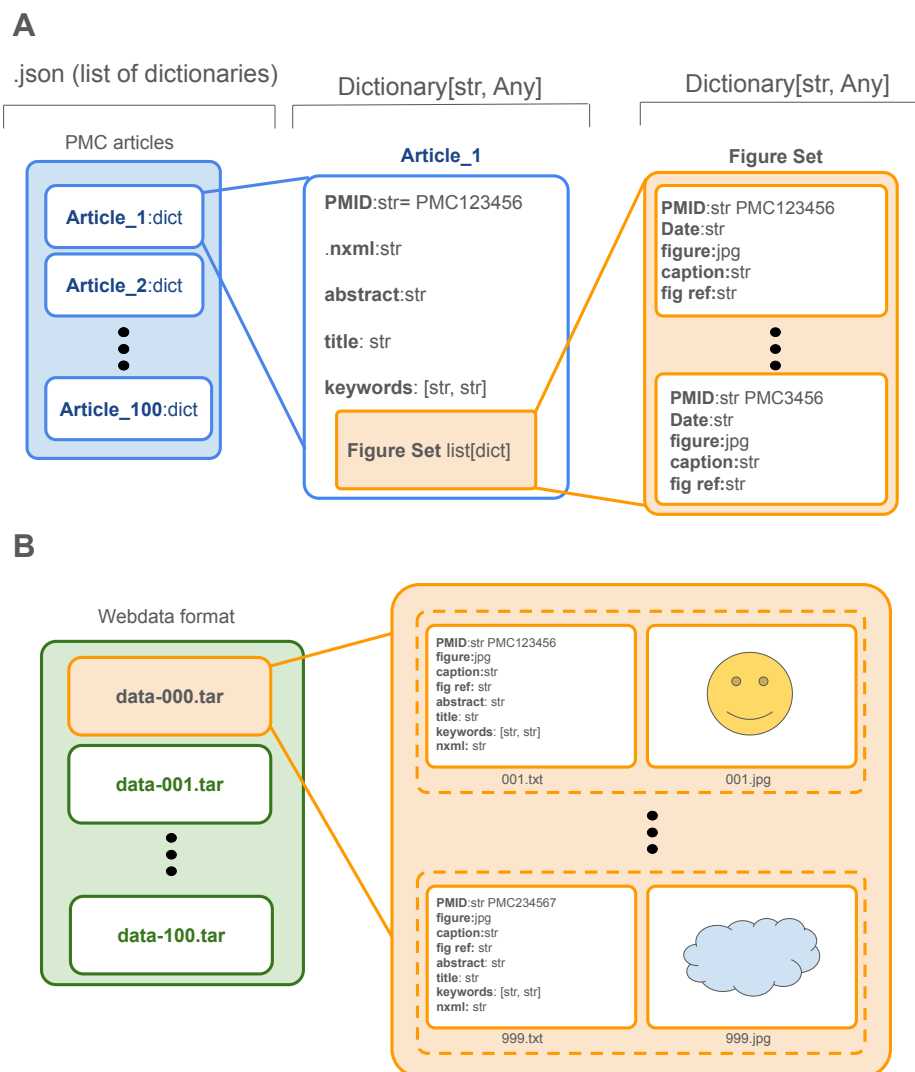


Figure 6. A) Diagram illustrating the structure of a JSON file containing a list of dictionaries representing PMC articles. Each article dictionary includes metadata fields such as PMID, nXML path, abstract, title, keywords, and a nested figure set. The figure set is a list of dictionaries, where each dictionary contains the figure’s PMID, volume number, image file, caption, and context. B) Diagram illustrating the WebDataset format, where data is stored across multiple .tar archives (e.g., data-000.tar, data-001.tar). Each archive contains paired text and image files representing individual records.

the dataset by figure, such that a row (figure within a figure set) becomes a unique image-caption pair rather than an article. This implies that each image-caption includes all the corresponding metadata. Note that this comes with the disadvantage of repeated entries for images belonging to the same figure set (e.g. within the same publication). In other words, if two different images come from the same article figure set, then all the metadata and nxml will be repeated twice. Figure 6 shows the data structure before (A) and after (B) serialization.

PMC-OA Subsets were serialized in parallel. Table 8 shows the total serialization run time. Notably, we can serialize the entirety of PMC-OA within a single day.

13.4. Tokenized Caption Distribution

Note that the histogram in Figure 9 shows a long right tail in the distribution of caption token lengths, with many captions exceeding the CLIP model’s context length limit. **Need to provide numbers, mean min, max, median etc**

This issue is even more pronounced for figure reference.

Subset	Serialization Time (Hrs)
Commercial	23:50:57
NonCommercial	7:36:35
Other	1:36:42
Total	33:04:14

Table 8. Total Serialization time by PMC-OA subset

14. Concept Labeling: Additional Details

We developed an AI-assisted pipeline to categorize similar concepts within PMC-OA, as described in section Section 3.2. In summary, this process involves four stages: First, we define and organize similar images in clusters applying unsupervised clustering on image content, second, a group of 2 clinicians and 1 scientist use these clusters and taxonomies to create a hierarchical taxonomy for PMC-OA (see Figure 10), then a group of 2 clinicians and 6 scientists use this taxonomy to annotate each cluster. A majority vote approach is used to select the final cluster annotations. Lastly, this metadata is propagated to each cluster instance.

In this section, we provide additional details and experiments for each design choice.

14.1. Dimensionality Reduction

We used DINOv2 (ViT-L/14 distilled) to generate a 1024-dimensional vector for each image in PMC-OA. However, directly clustering such high-dimensional data can lead to poor performance due to the "curse of dimensionality," where the increased sparsity in high-dimensional spaces reduces the reliability of distance-based measures like those used in K-means clustering.

To address this, we applied PCA (Principal Component Analysis) to reduce the dimensionality of the embeddings. A scree plot analysis was performed to determine the minimum number of principal components required to retain 99% of the data variance. As shown in Table 7, 25 principal components were sufficient to achieve this threshold. Consequently, we selected PCA (n=25) to transform the data before applying K-means clustering.

14.2. Over-Clustering

We opt to over-cluster using KMeans with (K=2000), as this approach allows us to thoroughly explore the PMC-OA dataset. By focusing on fine-grained patterns and subgroups, this strategy ensures a detailed analysis, particularly when the optimal number of clusters remains uncertain. This number was also selected to achieve an effective annotation time of at most **72 hours per annotator**.

To do this at scale, we extract DINO-v2 features in parallel with NVIDIA Triton Inference. PCA and K-means are

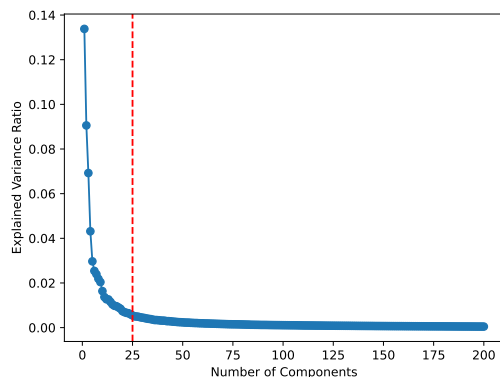


Figure 7. DinoV2 features Scree plot

not parallelized. However, due to the simplicity of these approaches, they scaled to 24M pairs. Finally, cluster labels are stored along with image-uid. This is later used to propagate metadata to individual instances.

14.3. Online Cluster Annotations Form

Via a form hosted on Google Forms we asked two practicing clinicians and 5 scientists to annotate each image cluster by answering the following questions:

1. *Are the majority images within this cluster single panel or multiple panel?* Options:
 - Single Panels
 - Multiple panels with non-biomedical imaging
 - Multiple panels with biomedical imaging and plots
 - Multiple panels with biomedical imaging and assays
2. *Think of the main characteristics the MAJORITY of images in this cluster share in common. Given these characteristics, what is the most likely global class for this group?* Options:
 - Clinical Imaging
 - Microscopy
 - Immuno Assays
 - Illustrative Diagrams
 - Hand Drawn and Screen Based Visuals
 - Tables
 - Plots and Charts
 - PCR
 - Graph and Network
 - Scientific Formulae and Equations
 - Chemical Structures
 - Maps
 - Tools and Materials
3. *Given these characteristics, what is the most likely local class for this group? (remember to use the hierarchical taxonomy provided)*

Due to the quantity of high-resolution images, is not possible to compile all clusters together, thus 20 Google Forms, each containing 100 clusters were automatically created using Google Apps Script. Within each form, we provide the cluster image on top of each question to facilitate annotations. Annotators are calibrated by doing a practice run on 20 examples (these annotations are not added to the analysis). Annotators were given two weeks **336 hours** to fill all assigned forms. Annotators could only be assigned up to 1000/2000 clusters (10 forms). Lastly, forms were overlapped with a maximum of three annotators, meaning that annotations could have at most three labelers.

14.4. Taxonomy Curators Statistics

Table 15 shows statistics for taxonomy curators (denoted with *). Curators have a minimum of 3 years of experience, with a median of 11 years and a maximum of 14 years. Both clinical curators have an additional PhD. All curators have wet-lab experience.

14.5. Cluster Annotator Statistics

Table 15 shows statistics for cluster annotators. Annotators have a minimum of 3 years of experience, with a median of 4 years and a maximum of 14 years. On average, annotators spent 17.66 hours to finish all assigned forms. Collectively, annotators spent 103 hours annotating all 2000 clusters.

For our statistics, experience in the biomedical domain is measured from the time a person starts their graduate studies (such as a master’s or Ph.D.) and continues to accumulate as they work in the field. For this work, undergraduate studies do not contribute to the experience count, meaning that time spent pursuing a Bachelor’s degree or any other undergraduate-level studies is excluded from the total experience calculation, even when it’s biomedical related.

14.6. Dataset Taxonomy

The full delivered taxonomy is shown in Figure 10. Examples of topics with their corresponding image cluster are shown in Table 18. In total the taxonomy spans 13 global topics enumerated below:

- Clinical Imaging
- Microscopy
- Plots and Charts
- Immuno Assays
- Illustrative Diagrams
- Scientific Formulae and Equations
- Tables
- Hand Drawn and Screen Based Visuals
- Graph and Network
- Chemical Structures
- Maps
- Tools and Materials

- PCR (Polymerase Chain Reaction)

Notice that in contrast to the derived taxonomy, "Clinical and Scientific Image Data" is not included as a topic. Instead we itemize this concept by its children (clinical imaging and microscopy). This design choice facilitates labeling. For the rest of this work, clinical imaging and microscopy do not share any parent.

14.7. Label Assignment and Propagation

After labeling, each cluster has at most three expert-level annotations pertaining to panel type, global taxonomy, and local taxonomy. To resolve annotations, we follow a three-step pipeline:

1. Text Preprocessing Since panel-type and global taxonomy are multiple-choice questions, no further reprocessing is necessary. Local taxonomy, however, consists of open questions (users are asked to follow the taxonomy as shown in Figure 10). To this end, answers in this section are preprocessed by being lowercased, and white spaces and dashes are deleted.

2. Majority vote After preprocessing the final label for each field is resolved by taking the consensus of annotations by using the majority vote.

3. Label Propagation The metadata for the labeled cluster is then propagated to each image within that cluster. This is accomplished by retrieving the cached cluster label and image-uid (see Over-Clustering section) along with the corresponding resolved clustered metadata and adding this information to each item in within the serialized data.

Concept	Min	Max	Mean	Median	IQR
Panel	0.0	66.66	13.54	0.0	33.33
Global	0.0	66.66	8.39	0.0	0.0
Local	0.0	75.0	19.91	0.0	50.00

Table 9. Statistical overview of inter-annotator disagreement (lower is better).

14.8. Inter-annotator Disagreement

Table 9 shows a statistical overview of inter-annotator disagreement. The median disagreement for all concepts is 0.0, while the maximum disagreement (present in local taxonomy) is 19.91%, highlighting a high inter-annotator agreement greater than 80% for all concepts. 'Easier' concepts, such as global taxonomy, show a low mean disagreement of 8.39%. Figure 8 shows a histogram summarizing these findings.

14.9. Data Upload

Data is uploaded to HuggingFace using "upload_large_folder" with 40 workers. This upload mecha-

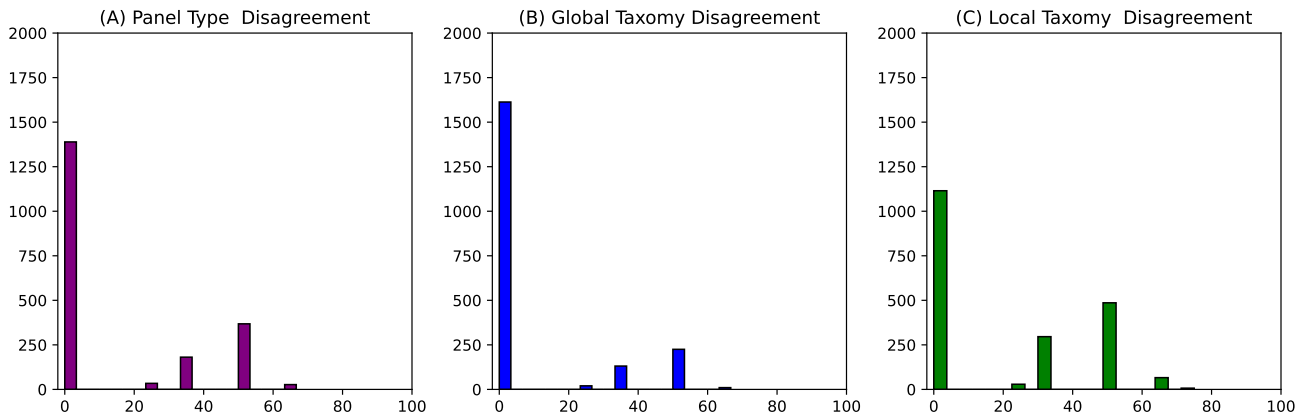


Figure 8. Inter-annotator disagreement (lower is better).

nism enables parallelism but relies on an already structured dataset.

```
from huggingface_hub import HfApi

api = HfApi(token=HF_TOKEN)
api.upload_large_folder(
    repo_type = "dataset",
    repo_id = REPO_ID,
    folder_path = LOCAL_PATH,
    num_workers = 40)
```

15. Model training

15.1. Base Model selection

In biomedical model development, it is common to skip ablations when selecting a strong base model for continual pretraining, often defaulting to models that yield state-of-the-art results in general domains. To this end, we use the validation sets of four random datasets to identify a robust base model for further fine-tuning (see Table 10). Our analysis reveals that, generally, ViT models trained on datasets such as CommonPool, Liabo2B, and WebLi achieve the strongest performance in the selected biomedical domains, while previously favored models like CoCa show the weakest results. Based on these findings, we select CLIP, ViT-L-14 Base as our model for subsequent experiments.

15.2. Modeling Hyperparameters

We detail the key configurations for training our model as follows:

- **Batch Size and Accumulation:** We use a batch size of 1024 per GPU on 4 GPUs with a batch accumulation frequency of 2, yielding an effective batch size of 8192.
- **Learning Rate:** We perform a sweep of learning rates from $1e-6$ to $1e-8$. We select the biggest learning rate

with stable training curve. To this end, We use a learning rate of $1e-6$ and a warmup phase of 1000 steps.

- **Optimizer:** We use the Adam optimizer with parameters set to $\beta_1 = 0.9$ and $\beta_2 = 0.95$, and a weight decay of 0.2.
- **Floating-Point Precision:** All computations are performed with 32-bit floating-point precision.

Table 11 summarizes all parameters used during training.

Model	Pretraining Dataset	Mean
ViT-L-14	commonpool	38.465
ViT-B-32	laion2b	37.892
ViT-SO400M-14-SigLIP	webli	35.010
ViT-L-14	laion2b	33.951
convnext-larged-320	laion2b	33.773
ViT-L-14	datacomp	33.148
EVA02-B-16	merged2b s8b b131k	32.995
RN50-quickgelu	openai	32.736
ViT-B-16-SigLIP-384	webli	32.482
ViT-B-16-SigLIP	webli	32.399
ViT-B-16-SigLIP-256	webli	31.762
EVA02-L-14	merged2b s4b b131k	31.680
ViT-B-16-SigLIP-512	webli	31.319
ViT-B-32	commonpool	30.614
coca-ViT-B-32	laion2b	29.133
ViT-B-32	datacomp	29.077
convnext-B	laion2b	28.701
ViT-B-16	laion2b	25.786
coca-ViT-L-14	laion2b	25.212

Table 10. Average Accuracy of Base Models (with Corresponding Pretraining Datasets) on 5 biomedical classification tasks

Model	Continual Training Data	Hyperparameters	Values
CLIP: ViT-L-14 (commonpool)	Full Data (24M)	batch size (per GPU)	1024
		GPUs	4xH100
		accumulation frequency	2
		effective batch size	8192
		learning rate	1e−6
		beta1	0.9
		beta2	0.95
		warmup	1000
		epochs	9
		precision	FP32
		gradient clipping norm	1.0
		dataset type	WebDataset
	Concept Balanced Data (8M)	batch size (per GPU)	1024
		GPUs	4xH100
		accumulation frequency	2
		effective batch size	8192
		learning rate	1e−6
		beta1	0.9
		beta2	0.95
		warmup	1000
		epochs	27
		precision	FP32
		gradient clipping norm	1.0
		dataset type	WebDataset
	Concept Filtered Data (6M)	batch size (per GPU)	1024
		GPUs	4xH100
		accumulation frequency	2
		effective batch size	8192
		learning rate	1e−6
		beta1	0.9
		beta2	0.95
		warmup	1000
		epochs	36
precision		FP32	
gradient clipping norm		1.0	
dataset type		WebDataset	

Table 11. Hyper-parameters used for continual pretraining.

Table 12. Provenance of evaluation benchmark. Each row lists dataset name (with its corresponding citation), task description, image modality, and number of classes in each corresponding tasks.

Dataset	Task	Modality	N. Classes
Cell Biology			
<i>Cell Cycle & Stage Identification</i>			
BBBC048 (BF) [19]	Cell cycle phase	Fluorescence Microscopy	7
BBBC048 (DF) [19]	Cell cycle phase	Fluorescence Microscopy	7
BBBC048 (EF) [19]	Cell cycle phase	Fluorescence Microscopy	5
<i>Cell Profiling</i>			
PCST Contour [10]	Cell contour	Fluorescence Microscopy	3
PCST-Texture [10]	Cell texture	Fluorescence Microscopy	3
PCST Eccentricity [10]	Cell eccentricity	Fluorescence Microscopy	3
<i>Cell & Structure Identification</i>			
Fluorescence Cells [38]	Organisms and structures	Fluorescence Microscopy	13
EMPIAR SBF-SEM [28]	Organisms and structures	Electron Microscopy	5
ICPR2020 Pollen [6]	Pollen structures	Fluorescence Microscopy	4
Pathology			
<i>Cytology</i>			
Acevedo et al 2020 [1]	White blood cell	Light Microscopy (Giemsa)	8
Jung et al 2022 [31]	White blood cell	Light Microscopy (Giemsa)	5
Pap Smear 2019 [24]	Pap smear grading	Light Microscopy (Pap Smear)	4
<i>Neoplastic Histopathology</i>			
Kather et al 2016 [32]	Colorectal tissue	Light Microscopy (H&E)	8
LC25000 (Lung) [8]	Lung tissue classification	Light Microscopy (H&E)	3
PCAM [35]	Lymph node classification	Light Microscopy (H&E)	2
LC25000 (Colon) [8]	Colon tissue classification	Light Microscopy (H&E)	2
<i>Non-neoplastic Histopathology</i>			
Tang et al 2019 [52]	Amyloid morphology	Light Microscopy (IHC)	4
Wong et al 2022 [57]	Amyloid morphology	Light Microscopy (IHC)	4
Nirschl et al 2018 [42]	Clinical chronic heart failure	Light Microscopy (H&E)	2
Wu et al 2023 [60]	Mitochondrial morphology	Light Microscopy (IHC)	2
General Microscopy			
Micro-Bench Submodality [38]	Microscopy Submodality	Microscopy	6
Micro-Bench Stain [38]	Microscopy Stain	Microscopy	6
Micro-Bench Domain [38]	Microscopy Domain	Microscopy	6
Micro-Bench Modality [38]	Microscopy Modality	Microscopy	3
Radiology			
<i>Diagnostics</i>			
Chexpert [27]	Chest X-Rays Findings	Chest X-Ray	5
RSNA 2018	Chest X-Rays Findings	Chest X-Ray	2
BreastMNIST [4]	Breast cancer diagnosis	Breast Ultrasound	2
Dermatology			
HAM1000 [54]	Common skin lesions	Dermatoscope	7
Surgery			
Dresden Anatomy Dataset [12]	Anatomy in surgery	Laparoscopic Surgery	7x2
Ophthalmology			
DeepDRiD [36]	Diabetic retinopathy	Retina Fundus Images	4

Text Statistics	Min	Max	Median	IQR	Total
Caption Token Length	4	1324	23	63	4.5×10^5
Caption Character Length	10	3287	78	149	1.10×10^6
Image Statistics					
Image Width (pixels)	70	1024	1024	1	
Image Height (pixels)	70	1024	768	87	
Image Area (pixels ²)	4900	1048576	786432	109206	

Table 13. Overview of Biomedical Flickr statistics, detailing text token and character lengths, and image dimensions. Tokens are generated using the BPE tokenizer from the `tiktoken` library

16. Evaluation

16.1. Closed VQA Benchmark

16.1.1. Closed VQA Formulation

A total of 39 existing classification tasks are formulated as multiple-choice visual question answering. The following subsection provides additional details for evaluation re-formulation.

We first collect the test set of each dataset, yielding image-label pairs.

$$D_i = \{(x_i^1, l_i^1), \dots, (x_i^{N_i}, l_i^{N_i})\}$$

where N_i corresponds to the total number of samples in the test subset of the i -th dataset.

For each image-label pair, the label l_i^j corresponds to one of M_i possible classes defined for the i -th dataset..

$$l_i^j \in C_i,$$

where $C_i = \{c_1, c_2, \dots, c_{M_i}\}$, $|C_i| = M_i$

To convert each classification task into a closed VQA task, we define a mapping function f_i for each dataset. This function maps a given label l_i^j to a human written textual description:

$$f_i : l_i^j \rightarrow t_i^j,$$

where t_i^j is the textual descriptor of label l_i^j . This process is applied to the entire dataset:

$$D_i = \{(x_i^1, t_i^1), \dots, (x_i^{N_i}, t_i^{N_i})\}$$

Then the remainder of (incorrect) classes textual descriptions are added to each data point to create a multiple-choice list: $A_i = \{t_i^j, a_i^1, a_i^2, \dots, a_{M_i-1}^i\}$. Lastly, a random permutation is applied, storing the position of the correct label after this operation k_i^j .

These operations convert the initial dataset to a collection of image-text pairs, where each image x_i is associated with: 1. A list of multiple-choice answers 2. The correct index of the label within this list, denoted as k_i :

$$D_i = \{(x_i^1, A_i^1, k_i^1), \dots, (x_i^{N_i}, A_i^{N_i}, k_i^{N_i})\}.$$

Where π denotes the random permutation function applied to the answers in $A_i^{\pi(j)}$.

16.1.2. Closed VQA Evaluation

All evaluated contrastive models have a vision encoder E_{image} and text encoder E_{text} . We first compute the image embedding, $z_{x_i} = E_{image}(\mathbf{x}_i^j)$, along with each candidate answer: $z_{a_i^{\pi(j)}} = E_{text}(a_i^{\pi(j)})$ for $l \in [1, M_i]$. Then we compute the cosine similarity score for each caption, $s_{ij} = z_{a_i^{\pi(j)}} \cdot z_{x_i}^T$ for $l \in [1, M_i]$. The option with the largest s_{ij} is then assigned as the final prediction. If $\text{argmax}(s_{ij})$ has the same index as the corresponding correct answer k_i^j the question is marked as correct, incorrect otherwise.

16.1.3. Closed VQA conversion prompts

If a dataset did not explicitly contain a Closed-VQA form, then a group consisting of a biomedical informatics, pathologist converted each class to unique its corresponding caption.

16.2. Retrieval Benchmark Evaluation

Given a dataset of images and captions

$$D_c = \{(x^1, c^1), \dots, (x^{N_i}, c^{N_i})\}.$$

We evaluate retrieval performance using Recall@k, using the following protocol:

All evaluated contrastive models have a vision encoder E_{image} and text encoder E_{text} . We first compute the image embedding, $z_{x_i} = E_{image}(\mathbf{x}^i)$, along with each caption: $z_{c_i} = E_{text}(c^i)$ for $l \in [1, M_i]$. Then we compute the cosine similarity score for each caption, $s_{ij} = z_{c_i} \cdot z_{x_i}^T$ for $l \in [1, N_i]$. Captions are arranged from the largest to smallest similarity (s_{ij}). If the correct caption is within the first k -th arranged items, then the option is considered relevant, irrelevant otherwise. lastly, we calculate Recall@k using the following equation:

$$\text{Recall@k} = \frac{\text{Number of relevant items in the top } k \text{ results}}{\text{Total number of relevant items in the dataset}}$$

16.3. Computing confidence intervals

Error bars represent 95% confidence intervals (CI) computed via nonparametric bootstrapping using the SciPy `stats.bootstrap` function with 1000 resampling and default settings.

17. Flickr Dataset Description

The Biomedical Flickr dataset consists of 7k image-caption pairs retrieved from flicker channels with permissive licenses. It mostly spans microscopy. Table 13 shows statistics for the dataset. Table 20 shows 10 random samples from the dataset.

18. Compute Environment

Experiments are performed in a local on-prem university compute environment using 24 Intel Xeon 2.70GHz CPU cores, 8 Nvidia H100 GPUs, 16 Nvidia A6000 GPUs, and 40 TB of Storage.

MeSH Term	Frequency
Humans	2,189,713
Female	990,873
Male	897,332
Animals	775,314
Adult	521,585
Middle Aged	483,806
None	375,532
Aged	371,170
Mice	288,320
Young Adult	205,580
Adolescent	200,700
Retrospective Studies	178,740
Child	166,187
COVID-19	149,167
Cross-Sectional Studies	135,551
Risk Factors	135,111
Treatment Outcome	131,638
Aged, 80 and over	125,351
Signal Transduction	109,685
SARS-CoV-2	100,287
Cell Line, Tumor	100,154
Surveys and Questionnaires	98,150
Prospective Studies	96,729
Prognosis	89,765
Rats	89,433
Pregnancy	88,439
Child, Preschool	79,751
Mutation	79,073
Biomarkers	77,093
Disease Models, Animal	76,046
Cell Proliferation	75,080
Time Factors	75,034
Mice, Inbred C57BL	72,500
Infant	71,594
Pandemics	70,915
China	68,963
Algorithms	64,904
Neoplasms	64,674
Cohort Studies	64,563
Reproducibility of Results	62,995
Phylogeny	62,412
Prevalence	61,952
Apoptosis	61,057
Cells, Cultured	58,811
Cell Line	57,933
Gene Expression Profiling	57,680
Brain	57,472
Case-Control Studies	57,044
Quality of Life	56,170
Infant, Newborn	55,529

Table 14. Top 50 most common MeSH Terms and their frequencies

	Years of experience	Field of study	Role
Annotator 1	3	Developmental biology	PhD Student
Annotator 2	3	Microbiology	PhD Student
Annotator 3*	3	Biomedical Informatics	PhD Student
Annotator 4	5	Biomedical Informatics	PhD Student
Annotator 5	3	Genetics	PhD Student
Annotator 6	9	Biomedical Informatics	MD-PhD Student
Annotator 7*	11	Biomedical Engineering, Molecular Biology, Surgical Data Science, ML	Industry Director, Post-doc
Annotator 8*	14	Pathology, Cell biology, Neuroscience	Attending Pathologist, Post-doc

Table 15. Description of cluster annotators. Years of experience include years of research or laboratory experience in a biology/biomedical or microscopy related discipline. * Annotator developed taxonomy.

Category	Other	Commercial	Noncommercial	Total
Scientific Formulae and Equations	2,322	20,384	6,182	28,888
PCR	2,307	25,353	7,693	35,353
Tools and Materials	10,320	210,740	51,339	272,399
Maps	18,700	264,092	41,473	324,265
Hand Drawn and Screen Based Visuals	24,690	356,047	76,404	457,141
Graph and Network	26,453	415,737	83,470	525,660
Tables	26,190	269,384	343,455	639,029
Immuno Assays	38,055	651,339	215,238	904,632
Chemical Structures	92,881	839,082	196,119	1,128,082
Clinical Imaging	82,349	1,078,901	766,908	1,928,158
Microscopy	101,617	1,818,302	597,413	2,517,332
Illustrative Diagrams	140,925	2,227,690	551,380	2,919,995
Plots and Charts	542,718	9,426,147	2,394,358	12,389,066

Table 16. Number of images by global taxonomy concepts.

License Type	Number of Articles
CC0	132592
CC BY	3795419
CC BY-SA	1287
CC BY-ND	7900
CC BY-NC	771755
CC BY-NC-SA	275638
CC BY-NC-ND	642982
Other	414857

Table 17. Number of articles by license type. As described in the PMC website: "Commercial use allowed: CC0, CC BY, CC BY-SA, CC BY-ND. Non-commercial use only: CC BY-NC, CC BY-NC-SA, CC BY-NC-ND. Other: no machine-readable Creative Commons license, no license tagged, or a custom license."

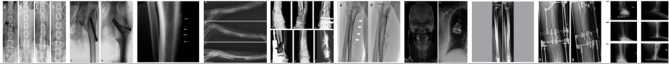
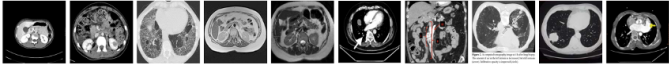
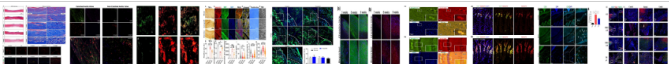
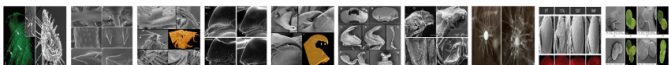
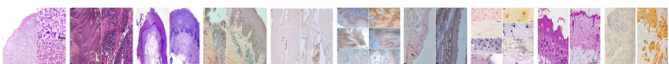
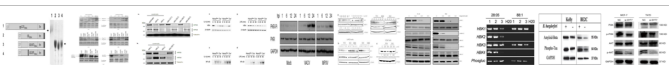
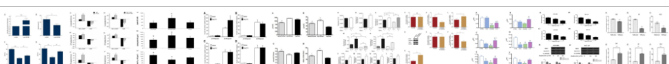
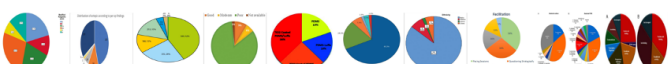
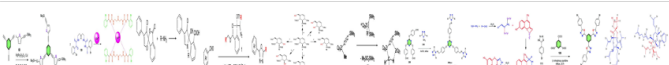
Cluster Example	Global Taxonomy	Local Taxonomy	Multi-panel
	Clinical Imaging Data	x-ray radiography	✓
	Clinical Imaging Data	computerized tomography	✓
	Clinical Imaging Data	electrocardiogram	✗
	Microscopy	fluorescence microscopy	✓
	Microscopy	electron microscopy	✓
	Microscopy	light microscopy	✓
	Immuno Assays	gel electrophoresis	✓
	Plots and Charts	bar plot	✓
	Plots and Charts	pie chart	✗
	Chemical Structures	2D chemical reaction	✗
	Chemical Structures	3D chemical structure	✗
	Illustrative Diagrams	signaling pathway	✗
	Tables	table	✗
	Maps	map	✗
	Drawings	drawing	✗
	Tools and Materials	lab equipment	✓
	Natural Images	natural image	✗

Table 18. Taxonomy of clusters with example images. Images resized to a uniform width of 10cm and height of 1cm. Column widths adjusted to fit the page.

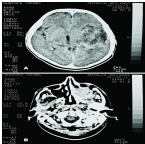
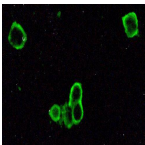
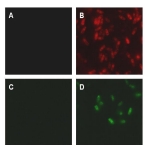
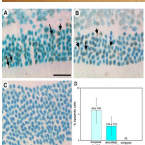
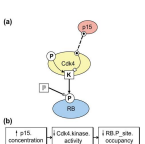
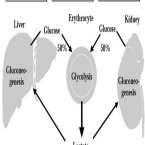
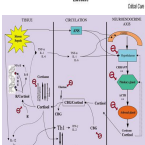
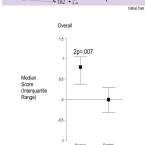
Image	Caption
	Four weeks after the accident: the radiograph shows good alignment (lateral view).
	CT-images belong to brain and maxillary sinus. Ct-images taken before any procedure applied illustrating two separate tumors in the brain (2a) and left-maxillary sinus (2b). Note the enhancing heterogeneous tumor at the left-temporoparietal lobe shifting the midline to the right (2a); and invasion of the tumor (T4) in the left-maxillary sinus into the adjacent tissues (2b).
	Detection of HSV-1 antigen. An impression cytology smear obtained from a patient with HSK showing the presence of rounded up corneal epithelial cells positive for viral antigen. Infected cells show brilliant apple green fluorescence. Note the absence of background staining. Indirect immunofluorescence assay, x 500.
	Detection of presence of CotC-LTB and CotC-TTFC by immunofluorescence microscopy. Sporulation of B. subtilis strains was induced by the resuspension method, and samples were taken 6 h after the onset of sporulation and analysed by immunofluorescence microscopy as described previously [46]. Samples were labelled with mouse anti-LTB antibody followed by anti-mouse IgG-TRITC conjugate (red fluorescein, Panels A & B), or rabbit anti-TTFC antibody followed by anti-rabbit IgG-FITC conjugate (green fluorescein, Panels C & D). Panels A & C, wild type spores; Panel B, isogenic spores expressing CotC-LTB); Panel D, isogenic spores expressing CotC-TTFC.
	Clinical photograph of the abdomen (close-up view): The surgical scar of implantation of baclofen pump is seen. The pigtail catheter emerges close to the scar. The skin around the pigtail catheter is red and angry-looking. Approximate position of baclofen pump is marked on the skin with a pen.
	Comparison of apoptotic cells numbers Photomicrographs of the outer nuclear layer of 8 mo uninjected Rpe65 ^{-/-} (A), rAAV.RPE65 injected Rpe65 ^{-/-} (B) and C57BL/6J mice (C) stained for apoptotic nuclei (arrows). (D) Graphical presentation of the percentage of photoreceptor nuclei that are apoptotic in uninjected Rpe65 ^{-/-} , rAAV.RPE65-injected Rpe65 ^{-/-} and uninjected C57BL/6J mice. Apoptotic and total photoreceptor nuclei were counted along 60 μm lengths of the outer nuclear layer of mice at 7 mo post-injection (8 mo of age). Average total photoreceptor counts: uninjected Rpe65 ^{-/-} = 106.8 ± 22.9, rAAV.RPE65 injected Rpe65 ^{-/-} = 134 ± 30.3, uninjected C57 = 213.5 ± 3.3. All data are mean ± S.D.
	Flow diagram showing randomisation and response rates of the survey.
	(a) A simplified model of a Cdk4 kinase molecule illustrates how basic BioD icons and action arrows can concisely represent intra- and inter-molecular actions. The Cdk4 molecule includes a kinase site (K) that, when active, phosphorylates a phosphorylation site (P) on the RB protein. The kinase site on Cdk4 is activated (filled arrow) by occupancy of its phosphorylation site and inhibited (open-squared arrow) by occupancy of the binding site (dotted circle) that binds the Cdk4 inhibitor p15. (b) An 'event model' derived from the model above. Events are defined as changes of state of one or more functional properties of icons in a state model. Here, for instance, the event model displays a chain of events triggered by an increase of p15 concentration (see text).
	Renal contribution to endogenous glucose release from lactate during the postabsorptive phase. Data from [1].
	Strategy for detection and treatment of adrenal failure during sepsis. ACTH, adrenocorticotrophic hormone.
	Mammographic changes in treated and control individuals. Values are expressed as median change from baseline and interquartile range.

Table 19. Biomedica dataset Image-caption examples Benchmark Example: 10 examples from Biomedica dataset grouped by concept

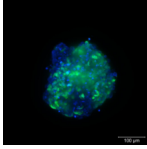
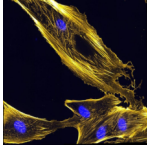
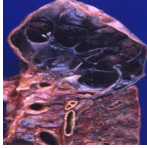
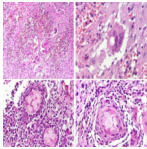
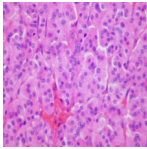
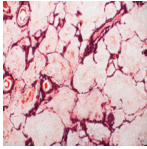
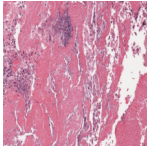
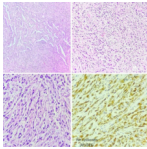
Image	Caption
	Colorized scanning electron micrograph of a cell (red) heavily infected with SARS-CoV-2 virus particles (green), isolated from a patient sample.
	HBE human derived cell lines cultured as micro-tissues (DAPI staining in blue; fixed with PFA). Infection with human Adenovirus type 2 expressing GFP.
	Immunofluorescence image of actin bundles in muscle precursor cells called myoblasts. The actin is labeled with fluorescently-tagged phalloidin, which is a toxin from the Amanita phalloides mushroom. Nuclei are shown in blue.
	Cut surface of a large apical bulla. Involved hilar lymph nodes also present.
	In this pleural biopsy, a chronic inflammatory reaction with giant cells is seen, reacting to the presence of food material originating from an esophageal fistula. In the two bottom photographs, the structure of this material, although deteriorated, is still preserved. These are particles of vegetable material which, due to their size and shape, surely are seed-derived storage cells.
	Typical carcinoid tumor with organoid/insular growth and oncocytic tumor cells. There are many morphologic variants of carcinoid tumors.
	Metastatic calcification of alveolar walls and blood vessels in an area of acute pneumonitis.
	Microfilarium
	Pleomorphic lung carcinoma is composed of 10% or more of spindle cells and/or giant cells admixed with variable amounts of adenocarcinoma, squamous carcinoma, or large cell carcinoma. Some are composed solely of spindle cells and/or tumor giant cells. The diagnosis can only be made in a surgical specimen, not in a biopsy specimen. The type(s) of non-spindle cell carcinoma that are present should be mentioned in the pathology report. The term "sarcomatoid carcinoma" should be avoided because it is an umbrella term encompassing pleomorphic carcinoma, carcinosarcoma, and pulmonary blastoma. These images of pleomorphic carcinoma show malignant spindle cells admixed with adenocarcinoma
	Normal PA chest x-ray

Table 20. BiomedFlickr Benchmark Example: 10 Random examples from biomedflickr

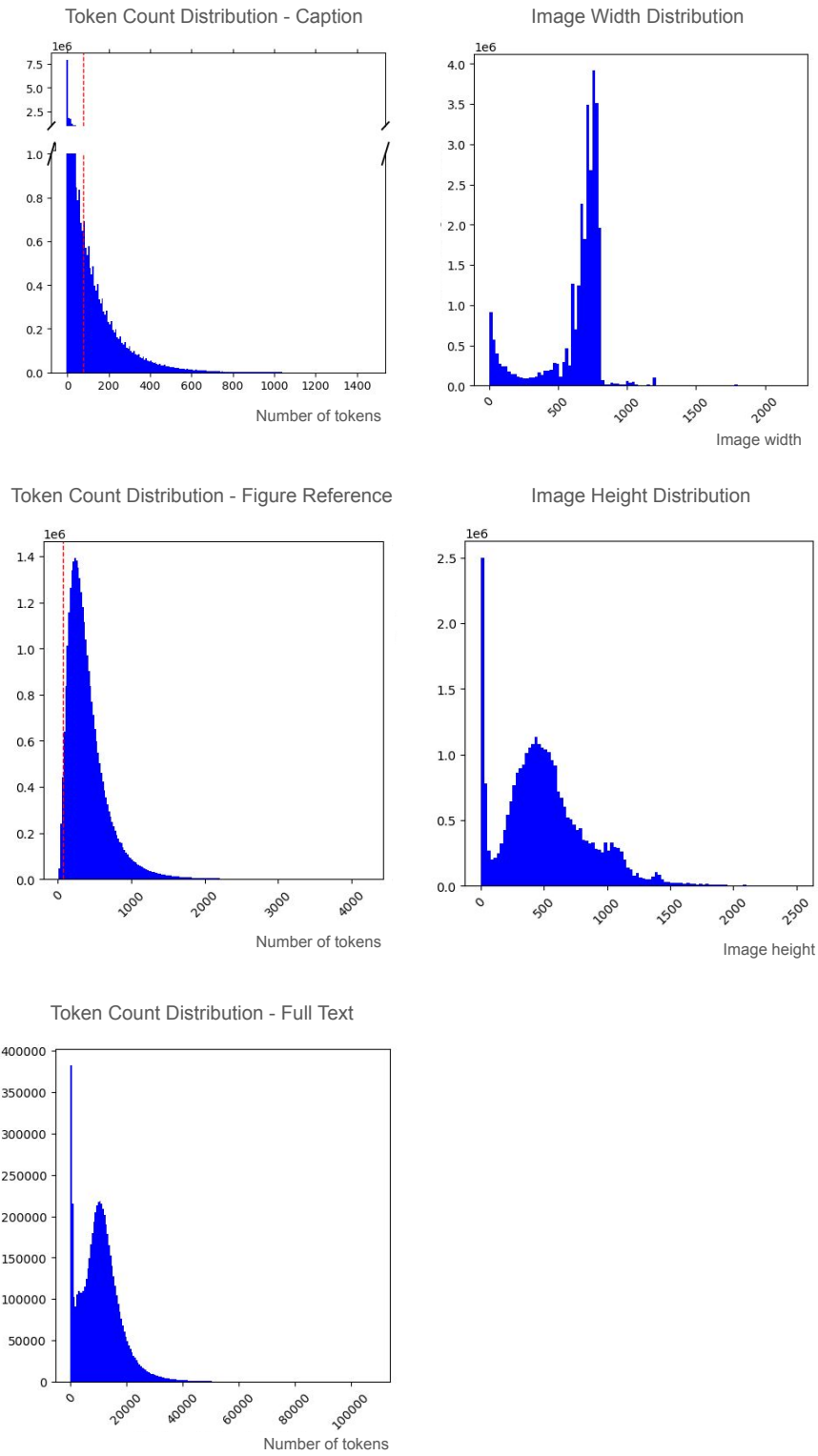


Figure 9. Distributions of token counts and image dimensions in the dataset. Histograms are shown for token counts in captions, figure references, and full text, as well as for image widths and heights. Outliers have been excluded to highlight the central tendencies and areas of higher data density.

```

TAXONOMY = {'Ambiguous': ['ambiguous'],

'Chemical Structures': ['2D chemical reaction', '3D chemical reaction', '2D chemical structure',
                        '3D protein structure', '3D chemical structure'],

'Clinical Imaging': ['x-ray radiography', 'optical coherence tomography', 'endoscopy',
                    'intraoral imaging', 'angiography', 'procedural image', 'skull', 'patient photo',
                    'functional magnetic resonance', 'magnetic resonance', 'eye', 'mammography',
                    'electrocardiography', 'clinical imaging', 'skin lesion', 'ultrasound',
                    'specimen', 'computerized tomography', 'laryngoscopy', 'teeth',
                    'intraoperative image', 'surgical procedure', 'brain'],

'Graphs and Networks': ['graph', 'neural network', 'network'],

'Illustrative Diagrams': ['sankey diagram', 'metabolic pathway', 'scientific illustration', 'diagram',
                          'signaling pathway', 'illustrative diagram', 'flow diagram',
                          'cohort selection flowchart', 'illustration', 'drawing', 'system diagram',
                          'flowchart'],

'Immuno Assays': ['immunocytochemistry', 'karyotype', 'gel electrophoresis', 'immunoassay',
                  'immunoblot', 'assay', 'immunohistochemistry'],

'Laboratory Specimens and Cultures': ['reagents', 'laboratory specimen', 'bacterial culture'],

'Maps': ['map'],

'Microscopy': ['scanning electron microscopy', 'electron microscopy', 'flowcytometry',
               'transmission electron microscopy', 'light microscopy', 'fluorescence microscopy',
               'phase contrast microscopy', 'confocal microscopy', 'epifluorescence microscopy',
               'microscopy'],

'Natural Images': ['face', 'aerial photography', 'natural image', 'human head', 'humans and devices',
                  'human', 'insects', 'nature'],

'PCR': ['qPCR', 'RT PCR'],

'Plots and Charts': ['violin plot', 'bar plot', 'roc curve', 'sequence plot', 'radial plot', 'plot',
                    'matrix plot', 'phylogenetic tree', 'process chart', 'dot plot', 'pyramid chart',
                    'forest plot', 'box plot', 'survival curve', 'circos plot', 'venn diagram',
                    'heatmap plot', 'circular plot', 'scatter plot', 'word cloud', 'list', 'tree',
                    'density plot', 'funnel plot', 'plot and chart', '2D mesh', '3D plot',
                    'radial diagram', 'pie chart', 'manuscript', 'histogram',
                    'differential gene expression matrix', 'line plot', 'signal plot'],

'Screen Based Visuals': ['screenshot', 'user interface'],

'Scientific Formulae and Equations': ['algorithm'],

'Tables': ['table', 'checklist table'],

'Tools and Materials': ['medical equipment', 'microscope', 'electronic circuit', 'lab equipment',
                       'tool']}

```

Figure 10. Hierarchical Taxonomy